Chapter

Some Research Method about Superconducting Magnet Systems of TOKAMAK

Jian Rong

Abstract

The superconducting magnet operates in conditions of complex electromagnetics, which could cause hysteresis loss and coupling losses, the so-called AC losses. In this chapter, the AC losses calculation of superconductor will be discussed in detail. Usually, the superconducting magnets are wound by superconducting coils, which are twisted by superconducting wires. The length of superconducting wires is hundreds of meters, while the length of coils is millions of meters; thus, joints are needed to join the coils. The design of different patterns of joints, such as twin-box joint, butt joint, and petal overlap joint, will be introduced in detail. Joule heat and AC losses in the joint may cause locality quench, and if the design stability margin of the magnet could not cover the joule heat and losses, the locality quench will cause global quench of the magnet. The temperature rise caused by joule heat and AC losses will be discussed in detail. Furthermore, the magnetic Lorentz force and mechanical displacement could cause locality quench, which may cause a global quench, once the coolant could not take away the heating pulse. The simulation of the stability and quench behavior of the superconducting cable-in-conduit conductor will be introduced in detail.

Keywords: AC losses, hysteresis loss, coupling losses, superconducting joint, current sharing temperature, temperature margin, minimum quench energy, hotspot temperature

1. Introduction

The TOKAMAK (toroidal, kamera, magnet, kotushka) is a typical magnetic confinement fusion device, which uses a powerful magnetic field to confine plasma in the shape of a torus. Long-time plasma confinement is needed for commercial electricity of tokamak, the superconducting magnet system could provide a long-time stable confinement field for the plasma of tokamak, and the plasma could operate a long time stably. Thus, the superconductivity is considered one of the key technologies to reach commercial electricity for tokamak.

There are two key components (superconducting CICC (cable-in-conduit conductor) and superconducting joints) in the superconducting magnet system. Superconducting CICC design refers to twist pattern, superconducting filament,
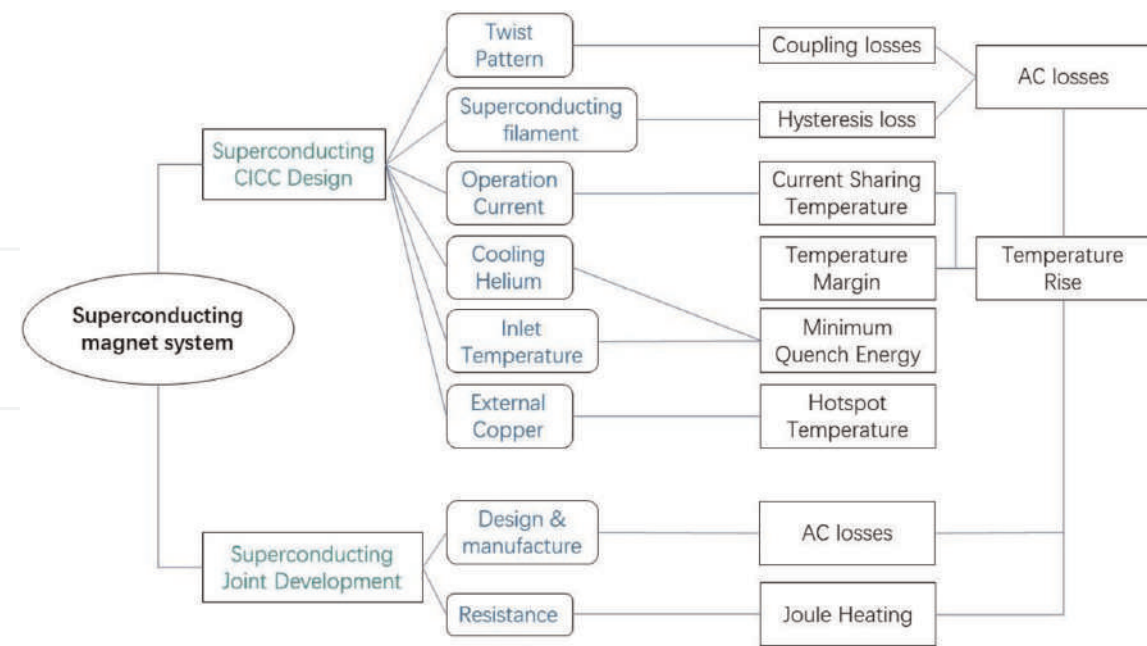
IntechOpen

Figure 1.
The chapter structure diagram.

operation current, cooling helium, inlet temperature, external copper, and so on, while superconducting joint design refers to the design, manufacture, and resistance, as shown in **Figure 1**. In this chapter, this factor of the CICC and joint design will be introduced in detail.

In the complex varying electromagnetic environment, the changing magnetic field could produce AC losses (include hysteresis loss and coupling losses) in the superconducting conductor and joints, which could cause a quench. The coupling losses are affected by the twisted pattern of the conductor, while the superconducting filament decides the hysteresis loss. AC losses and joint resistance will cause a temperature rise, which reduces the temperature margin, the cooling helium and inlet temperature decide the minimum quench energy, and the hotspot temperature is decided by the external copper. In this chapter, AC losses, current sharing temperature, and joint resistance calculation method will be introduced in detail, taking ITER TF (Toroidal Field) main busbar as an example, and its quench and stability behavior in 15 MA plasma current scenario will be discussed, which includes the temperature rise caused by AC loss and joint resistance, minimum quench energy, hotspot temperature. And a joint development design is introduced in detail, hoping that this chapter will help reader know how to study superconducting magnet system.

2. AC losses calculation of the ITER TF main busbar

A feeder system is used to supply the electrical power, cryogens, and control system interfaces outside the cryostat through a warm-cold barrier to the ITER magnets. Each feeder consists of control cubicles, Dry Box (DB), Coil Terminal Box (CTB), Pressure Release Valve Rack (PRVR), S-Bend Box (SBB), Cryostat Feed Through (CFT), and In-Cryostat Feeder (ICF) [1], as shown in **Figure 2**. The main busbar of the TF feeder is a kind of typical superconducting CICC, which employs 900 Ni-plated NbTi strands and 522 Ni-plated copper strands, and the pattern of the main
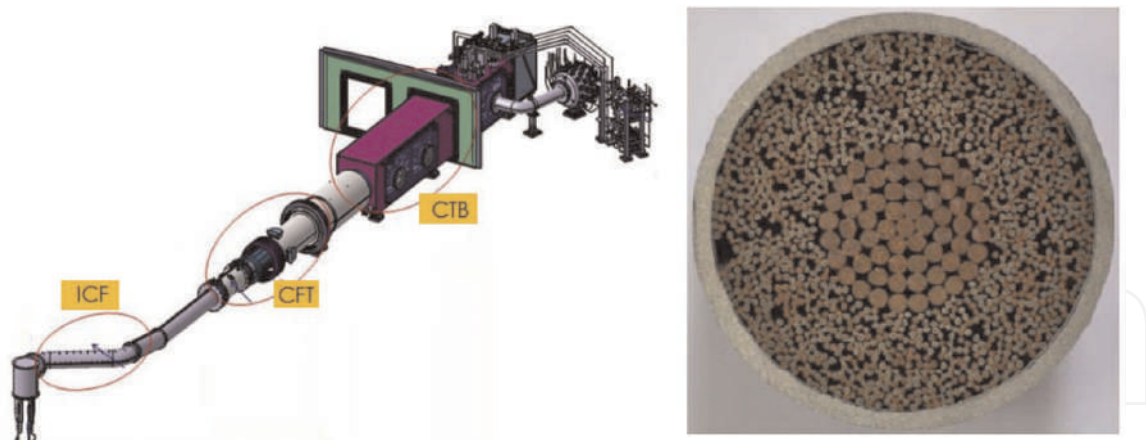
Figure 2.
The feeder system of the TF magnet of the ITER [2].

busbar conductor is (2SC + 1Cu) × 3 × 5 × (5 + C0) × (6 + C1), where C0 is 3 × 4Cu, and C1 is (1 + 6 + 12 + 18 + 24)Cu, and the sub-cables show petal structure without wraps. The complex changing complex electric-magnetic causes AC losses in the main busbar conductor. In this section, the AC losses calculation of the main busbar will be introduced in detail.

2.1 The hysteresis loss calculation of ITER main busbar

In the varying magnetic field, the moving flux will deposit the magnetic energy in the superconductor so-called hysteresis loss. Because there is flux pinning in the superconductor, the flux overcomes the pinning potential energy and surface potential barrier and does work, thus the hysteresis loss is produced. There are following four main kinds of calculation methods of hysteresis loss [3]:

a. In the varying magnetic field, there is an induced current in the superconductor, the hysteresis loss could be calculated by calculation of energy flowing into and out of the superconductor, and the hysteresis loss equals the integration of the Poynting vector ($S = E \times H$) on the field loop, where the electrical field could be calculated by Maxwell's equation of $\nabla \times E = -dB/dt$.

b. The hysteresis loss could be calculated by integrating the point multiplication of current density and electrical field ($J \cdot E$).

c. The hysteresis loss could be calculated by integrating the magnetizing curve ($Q = M(H)dH$) in the varying magnetic field.

d. The hysteresis loss per unit volume equals the work of Lorentz force ($SP = (J \times E) \cdot v$), where the v is the velocity of movement of the flux.

In the superconducting strands, the pattern of superconductor is twisted superconducting filaments, then the second method is chosen to calculate the hysteresis loss of superconductor. The superconductor is equivalent into a cylinder, and the Bean's critical state model is used in hysteresis loss calculation [4, 5], in which

the field flux penetrates the superconductor fully, and the current density is critical current density of superconductor. According to classical electromagnet theory, hysteresis loss per unit volume equals the product of electrical field and critical current density ($Jc \cdot E$). In the condition that the background field flux penetrates the superconductor fully, the field direction is perpendicular to the axis of the cylindrical superconductor, and the electrical field direction is parallel to Z-axis, as shown in

Figure 3, H_θ and H_r stand for the component in the direction of $\vec{\theta}$ and $\vec{r}$ of magnet field intensity, respectively.

According to Maxwell's equation, the following equation could be given [6]:

$$\nabla \times \vec{E} = -\mu_0 \frac{\partial \vec{H}}{\partial t} = \begin{vmatrix} \vec{e_r} & \vec{e_\theta} & \vec{e_z} \\ \frac{\partial}{\partial r} & \frac{1}{r}\frac{\partial}{\partial \theta} & \frac{\partial}{\partial z} \\ 0 & 0 & E_z \end{vmatrix} \rightarrow \begin{array}{l} \frac{1}{r}\frac{\partial E_z}{\partial \theta} = -\mu_0 \frac{\partial H_r}{\partial t} \\ \\ \frac{\partial E_z}{\partial r} = -\mu_0 \frac{\partial H_\theta}{\partial t} \end{array} \tag{1}$$

Where E_z equals $\left|\vec{E}\right|$, is the component of $\vec{E}$ in the Z-axis direction. Once H_r and H_θ are replaced by H, the Eq. (1) could be turned into the following equation:

$$\begin{array}{l} \frac{1}{r}\frac{\partial E_z}{\partial \theta} = -\mu_0 \frac{\partial H}{\partial t} sin\theta \\ \\ \frac{\partial E_z}{\partial r} = -\mu_0 \frac{\partial H}{\partial t} cos\theta \end{array} \tag{2}$$

Solve the Eq. (2), the following equation could be given:

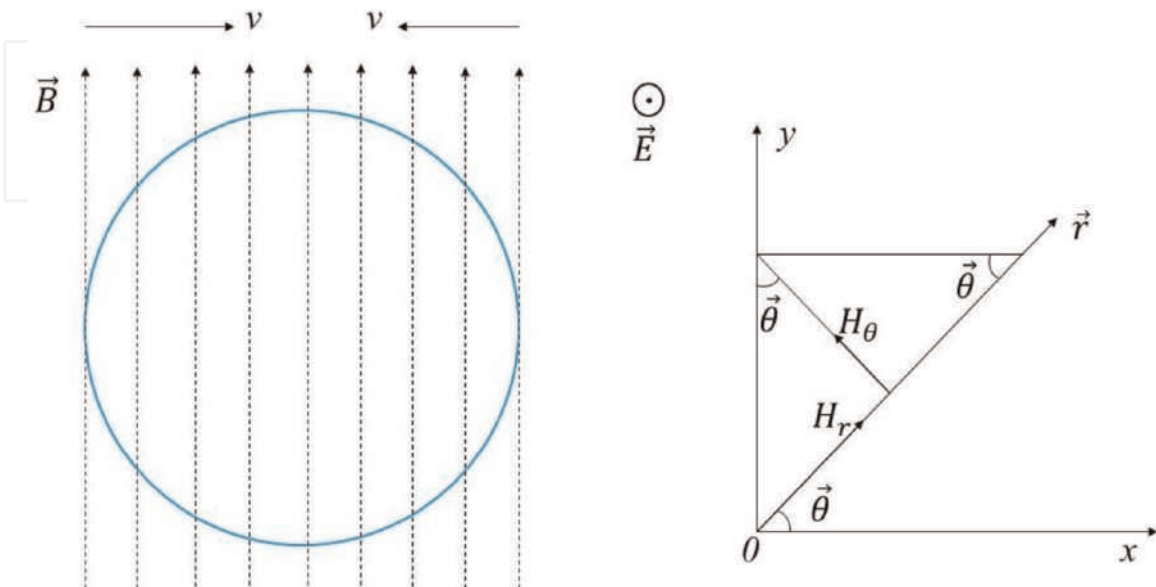$$E_z = \mu_0 \frac{dH}{dt} rcos\theta = \frac{dB}{dt} rcos\theta, \tag{3}$$

Figure 3.
The flux penetrates the cylindrical superconductor in the varying magnetic field, where v is the velocity of the flux moving into and out of the superconductor.

Then the hysteresis loss per unit length could be got in a polar coordinates system:

$$P = \int_S \vec{J} \times \vec{E} dS = 4 \int_0^{\frac{d_f}{2}} J_c \frac{dB}{dt} r^2 \cos\theta dr d\theta = \frac{1}{6} J_c \frac{dB}{dt} d_f^3.$$ (4)

Then the hysteresis loss per unit volume is given as the following (W/m^3):

$$P = \frac{2}{3\pi} \frac{dB}{dt} J_c d_f$$ (5)

Then the hysteresis loss of superconducting CICC per unit length is carried out by the following equation (only the loss when the magnetic field is perpendicular to the axis of a superconductor is considered) (W/m):

$$P_h = \frac{2}{3\pi} \frac{dB}{dt} J_c d_f A_{sc},$$ (6)

Where Jc is the critical current density of the superconductor, d_f is the effective diameter of the superconducting filament, A_{sc} is the total area of the superconductor, and dB/dt is the variation of the magnetic field. The effective diameter of a superconducting filament is affected by the connection between filaments, and the effective diameter is determined by experiment only, the effective diameter of a superconducting filament equals the average diameter of the filament during hysteresis loss calculation.

There are superconductors and normal conductors in the CICC, and because of hysteresis loss, it is represented that there is small resistance in the CICC, thus there is a small current in the normal conductor. Therefore, if the critical current density of the CICC is higher than Jc, then the hysteresis loss is given as the following Eq. (W/m):

$$P_h = \frac{2}{3\pi} J_c \left(1 + \left(\frac{I}{J_c A_{sc}}\right)^2\right) d_f A_{sc} \frac{dB}{dt},$$ (7)

Where I is the current of the superconducting CICC.

The critical current density of NbTi superconductor is calibrated as the function of temperature and background field by Bottura fie [7, 8], shown as the following function:

$$J_c(B, T) = \frac{C_0}{B} (b)^{0.8} (1 - b)^{1.2} \left(1 - t^{1.7}\right)^{2.61} J_{cre}$$

$$b = \frac{B}{B_{c20}(1 - t^{1.7})}$$ (8)

$$t = \frac{T}{T_{c0}}$$

Where C_0 is the normalization constant of 43.125 T of NbTi, B_{c20} is the upper critical magnetic field flux density with the temperature of 0 K, T_{c0} is the critical

temperature with the magnetic field of B = 0, and J_{cre} is the normalized value of critical current density at field 5.0 T and temperature 4.2 K (2800 A/mm^2) in the condition of NbTi superconductor.

The parameters of TF main busbar CICC of ITER are listed in **Table 1**, the diameter of the superconducting filaments is 8 μm, and the total cross-sectional area of the superconductor is 111.2 mm^2. In the reference scenario of 15 MA plasma current, the maximum magnetic field of the main busbar is 1.887 T and the minimum is 0.045 T, and the maximum variation of the magnetic field is 0.18 T/s. According to Eq. (7), the hysteresis loss is carried out, and the maximum value is 0.185 W/m. There is induced

Parameters		Value	Unit
Current	I	68	kA
Ratio of Cu to no-Cu of the strand	λ	2.35	mm^2
Radius of copper core zone of strand	r_c	0.175	mm
Radius of filamentary zone of strand	r_f	0.313	mm
Radius of copper shell zone of strand	r_{ms}	0.363	mm
Radius of the strand	R_0	0.365	mm
The diameter of the superconducting filament	d_f	8	μm
Thickness of Nickel plating	e_b	2	μm
Residual Resistivity Ratio of Ni and copper	RRR	100	
Cable twist pitch: (strand)	p_0	15	mm
1st	p_1	45	mm
2nd	p_2	85	mm
3rd	p_3	145	mm
4th	p_4	250	mm
5th	p_5	450	mm
Number of superconducting strands	N_{SC}	900	
Number of copper strands	N_{Cu}	522	
Diameter of Copper-core C1	r_5	17.73	mm
Inner conduit diameter	R_5	41.0	mm
Stainless steel conduit thickness		2.0	mm
Superconducting cross section	A_{SC}	111.2	mm^2
Copper cross section	A_{Cu}	671.0	mm^2
The bundle helium cross section	A_{He}	416.32	mm^2
The central helium cross section	A_{cen}	49.38	mm^2
C1 void fraction	ϑ_{C1}	20.0	%
Bundle void fraction	ϑ_{bundle}	38.78	%
Total void fraction of the conductor	ϑ_{busbar}	35.2	%

Table 1.
Properties of the TF main busbar of ITER [9–11].

current in the copper strands and copper matrix, and the flowing induced current causes coupling losses in the main busbar, which will be discussed in detail in the next section.

2.2 The coupling losses calculation of the ITER TF main busbar

In the superconducting CICC, there are normal conductor strands, a normal conductor matrix, and high-resistance plating, in which the induced current flowing causes the coupling losses. During coupling losses calculation, the superconducting strand is treated as a homogeneous mixture, and the magnetic field is assumed uniform distribution in the superconducting strands [7].

In the varying magnetic field, there is a coupling current in the matrix, because of the twist of superconducting filament, and the twist pitch is much longer than the diameter of superconducting filaments, the direction of the coupling current is parallel to the background field, and is different to the normal eddy current, as shown in **Figure 4**.

As shown in **Figure 4**, the total area surrounded by twisted superconducting filament in the Y-Z plane is given by following equation:

$$S(z) = \int_0^z R_f \cos\left(\frac{2\pi x}{p}\right) dx = \frac{p}{2\pi} R_f \sin\left(\frac{2\pi z}{p}\right). \tag{9}$$
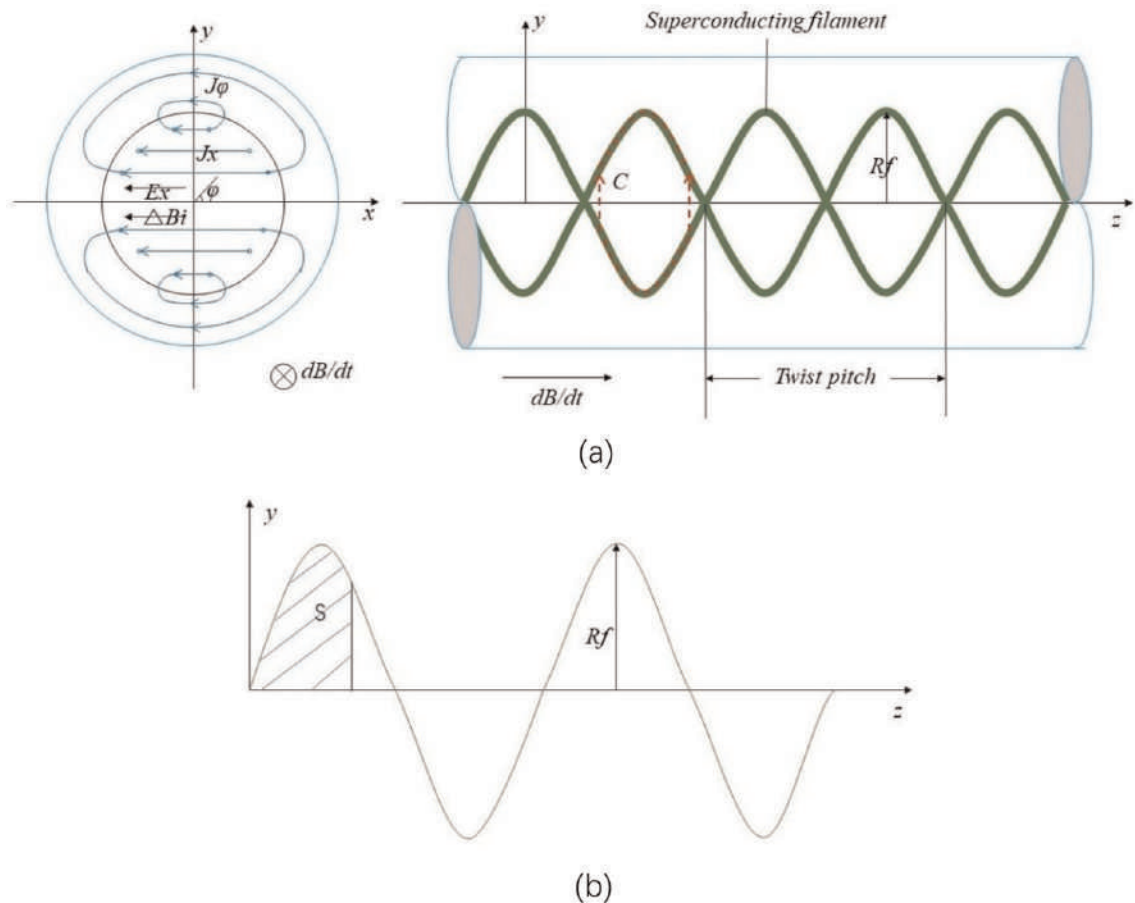

Figure 4.
The induced current in the superconducting filament and the area surrounded by the superconducting filament. (a) the induced current of the superconducting filament. (b) the area surrounded by the superconducting filament.

The induced electromotive force surrounded by C circuit in the Z direction, as shown in **Figure 4**, is given by following equation:

$$V(z) = \frac{-d\emptyset}{dt} = -S\frac{dB_i}{dt} = \frac{-p}{2\pi}R_f \sin\left(\frac{2\pi z}{p}\right)\frac{dB_i}{dt}, \tag{10}$$

Where p is the twist pitch of the superconducting filament, R_f is the radius of the twist zone, and the dBi/dt is the variation of the background magnetic field. Similarly, the induced electromotive force of X-direction in the cross section of superconducting filament could be determined by the following equation:

$$V(x) = \frac{-p}{2\pi}x\frac{dB_i}{dt}. \tag{11}$$

Then the average induced electric field strength is given by following equation:

$$\overrightarrow{E_x} = \frac{-p}{2\pi}\frac{dB_i}{dt}. \tag{12}$$

Then the transverse induced current density is given by following equation:

$$J_x = \frac{-p}{2\pi\rho_t}\frac{dB_i}{dt}. \tag{13}$$

Thus the transverse induced electric field strength is calculated by following equation:

$$E_x = J_x\rho_t = \frac{-p}{2\pi}\frac{dB_i}{dt}, \tag{14}$$

Where ρ_t is the transverse resistivity of the superconducting filament zone, and it is assumed that e is the thickness of the high resistivity layer around the superconducting filaments. The induced electrical field induces a current, whose direction is parallel to the induced electrical field, the current has an azimuth angle, and flows through a matrix. If $e \ll R_f$, the current density in an angular direction, as shown in **Figure 4**, is:

$$J_\varphi = \frac{-p}{2\pi\rho_n}\frac{dB_i}{dt}\sin(\varphi), \tag{15}$$

Where the ρ_n is the resistivity of the matrix out of the superconducting filaments zone, and φ is the angle between the axis of superconducting filaments and the background field shown in **Figure 4**.

The current density in the surface of superconducting filaments could be given by the correct balance current of transverse and angular induced currents:

$$J_x = \left(\frac{p}{2\pi}\right)\left(\frac{1}{\rho_t} + \frac{e}{R_f\rho_n}\right)\frac{dB_i}{dt}\sin(\varphi). \tag{16}$$

The coupling losses caused by the induced current flowing in the matrix of the superconducting strand is $P_c = J_x E_x$, generally, the angular φ equals to $\pi/2$, therefore,

the coupling losses of superconducting filaments zone are calculated by the following equation:

$$P_c = \frac{p}{2\pi}\left(\frac{1}{\rho_t}+\frac{e}{R_f\rho_n}\right)\frac{dB_i}{dt}\left(\frac{-p}{2\pi}\frac{dB_i}{dt}\right) = \left(\frac{1}{\rho_t}+\frac{e}{R_f\rho_n}\right)\left(\frac{p}{2\pi}\right)^2\left(\frac{dB_i}{dt}\right)^2. \tag{17}$$

A physical parameter that the coupling time constant of superconducting filament zone is defined:

$$\tau = \frac{\mu_0}{2}\left(\frac{1}{\rho_t}+\frac{e}{R_f\rho_n}\right)\left(\frac{p}{2\pi}\right)^2. \tag{18}$$

Because $e \ll R_f$, then relative $1/\rho_t$, $e/R_f\rho_n$ could be ignored, then the coupling time constant and coupling losses are shown by following equation:

$$\tau = \frac{\mu_0}{2\rho_t}\left(\frac{p}{2\pi}\right)^2, \tag{19}$$

$$P_c = \frac{2\tau}{\mu_0}\left(\frac{dB_i}{dt}\right)^2. \tag{20}$$

And the coupling losses per unit length superconducting conductor are shown by following equation:

$$P_c = \frac{2\tau}{\mu_0}\left(\frac{dB}{dt}\right)^2(1+\lambda)A_{sc}, \tag{21}$$

Where λ is the ratio of matrix and superconductor.

Generally, the superconducting strands are the composite structure of the normal conductor matrix and superconductor, the superconducting filaments twists in the strands immerse in the matrix. The superconducting strands consist of a normal conductor matrix, superconducting filament, a high resistivity layer, and a sheath around the strands, in which the superconducting filaments distribute evenly. The cross sections of superconducting strands are shown in **Figure 5**, and the cross-section
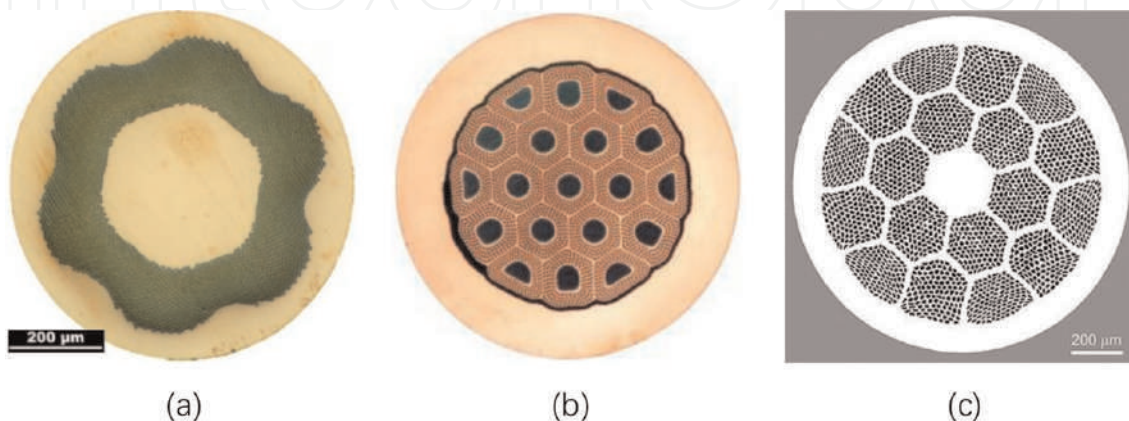

(a) (b) (c)

Figure 5.
(a) The cross section of NbTi strand of ITER main busbar [9], (b) the cross section of Nb3Sn strand of ITER TF coils (OST) [10], (c) the cross section of Bi-2212 round wire [12].

strand is divided into the core zone, superconducting filamentary zone, the matrix shell zone, high-resistivity layer, and sheath of the strands.

The cross section of superconducting strands is equivalent to several concentric circles during coupling losses of the strand calculation, the total coupling time constant of the strand is the sum of the time constant of all zones, as shown in the following equation:

$$\tau_0 = \tau_c + \tau_f + \tau_{mf} + \tau_b + \tau_{ms} + \tau_e, \tag{22}$$

Where τ_0, τ_c, τ_f, τ_{mf}, τ_b, τ_{ms}, and τ_e are the total time constant of the total strand, the time constant of the core zone, filamentary zone, filamentary shell zone, high resistivity layer, sheath of the strands, and the eddy current, respectively. According to Eq. (19), the time constant of each zone is given as follows [7, 13]:

a. The time constant of core zone:

$$\tau_c = \frac{\mu_0}{2\rho_{mc}} \left(\frac{p}{2\pi}\right)^2 \frac{r_c^2}{r_{ms}^2}, \tag{23}$$

b. The time constant of filamentary zone:

$$\tau_f = \frac{\mu_0}{2\rho_{tf}} \left(\frac{p}{2\pi}\right)^2 \frac{r_f^2 - r_c^2}{r_{ms}^2}, \tag{24}$$

c. The time constant of filamentary shell zone:

$$\tau_{mf} = \frac{\mu_0}{2\rho_{mf}} \left(\frac{p}{2\pi}\right)^2 \frac{r_{mf}^2 - r_f^2}{r_{ms}^2} \left(r_f^2 + b_1^2 r_{mf}^2\right) a_1^2, \tag{25}$$

d. The time constant of high-resistivity layer:

$$\tau_b = \frac{\mu_0}{2\rho_b} \left(\frac{p}{2\pi}\right)^2 \frac{r_f^2}{r_{mf}^2} \frac{r_b^2 - r_{mf}^2}{r_{ms}^2} \left(r_{mf}^2 + b_2^2 r_b^2\right) a_2^2, \tag{26}$$

e. The time constant of the sheath:

$$\tau_{ms} = \frac{\mu_0}{2\rho_s} \left(\frac{p}{2\pi}\right)^2 \frac{r_{mf}^2}{r_b^2} \frac{r_{ms}^2 - r_b^2}{r_{ms}^2} \left(r_{ms}^2 + r_b^2\right) a_3^2, \tag{27}$$

f. The time constant of the eddy current:

$$\tau_e = \frac{\mu_0}{8} \left(\frac{r_c^2}{\rho_{mc}} + \frac{\delta\left(r_f^4 - r_c^4\right)}{r_f^2 \rho_{tf}} + \frac{r_{mf}^4 - r_f^4}{r_{mf}^2 \rho_{mf}} + \frac{r_b^4 - r_{mf}^4}{r_b^2 \rho_b} + \frac{r_{ms}^4 - r_b^4}{r_{ms}^2 \rho_{ms}} \right), \tag{28}$$

Where the r_c, r_f, r_{mf}, r_b, and r_{ms} are the radius of core zone, filamentary zone, filamentary shell zone, high resistivity layer, and sheath of the strands, respectively; ρ_c,
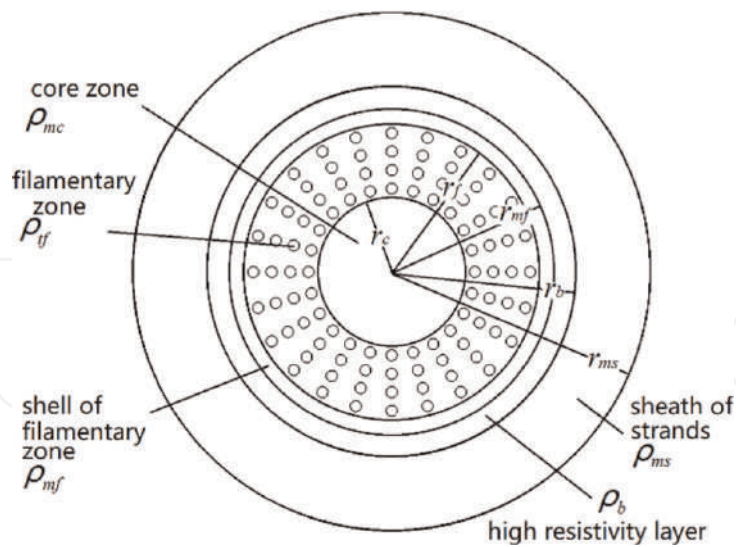
Figure 6.
The schematic layout of the cross section of the superconducting strand.

ρ_{mf}, ρ_b, and ρ_{ms} are the resistivity of core zone, filamentary shell zone, high-resistivity layer, and sheath of the strands respectively, as shown in **Figure 6**, and the δ is the ratio of the superconductor in the filamentary zone. In the previous equation, a_1, a_2, a_3, b_1, and b_2 are given by the following:

$$a_1 = \frac{r_f}{r_f^2 + b_1 r_{mf}^2}$$

$$a_2 = \frac{a_1(1 + b_1)r_{mf}^2}{r_{mf}^2 + b_2 r_b^2}$$

$$a_3 = \frac{a_2(1 + b_2)r_b^2}{r_b^2 + r_{ms}^2}$$

$$b_1 = \frac{\rho_b\left(r_{mf}^2 + b_2 r_b^2\right) + \rho_{mf}\left(b_2 r_b^2 - r_{mf}^2\right)}{\rho_b\left(r_{mf}^2 + b_2 r_b^2\right) - \rho_{mf}\left(b_2 r_b^2 - r_{mf}^2\right)}$$

$$b_2 = \frac{\rho_{ms}\left(r_{ms}^2 + r_b^2\right) + \rho_b\left(r_{ms}^2 - r_b^2\right)}{\rho_{ms}\left(r_{ms}^2 + r_b^2\right) - \rho_b\left(r_{ms}^2 - r_b^2\right)}$$

$$(29)$$

ρ_f and ρ_{tf} are the effective resistivity and equivalent resistivity, respectively, which are given by the following equation:

$$\rho_{tf} = \frac{(1 - \lambda)\rho_m + (1 + \lambda)\rho_f}{(1 + \lambda)\rho_m + (1 - \lambda)\rho_f}\rho_m$$

$$\rho_f = \frac{2R_{cmf}}{d_f}$$

$$(30)$$

Where ρ_m is the resistivity of the matrix in the filamentary zone, R_{cmf} is the contact resistance of filament-to-matrix, and λ is the ratio of a superconductor to the matrix in the superconducting filament zone, which is given by the following equation:

$$\lambda = \frac{A_f}{\pi\left(r_f^2 - r_c^2\right) - A_f}, \tag{31}$$

Where A_f is the cross-sectional area of the filamentary zone.

According to the need for cooling, support, and steady state, the magnet system of tokamak uses a CICC, in which the conductor is multistage cabled by superconducting and copper strands in a conduit carrying single-phase supercritical helium.

The total time constant of the conductor equals the sum of all contributions time constant [7]:

$$\tau = \sum_{n=0}^{N} \tau_n, \tag{32}$$

Where τ_0 is the time constant of the superconducting strand, τ_n is associated with the contribution of each cabling stage sub-cable ($n \geq 1$), which is calculated by following method:

$$\tau_n = \frac{\mu_0}{2\rho_n}\left(\frac{p_n}{2\pi}\right)^2 \frac{1}{1 - \vartheta_n}, \tag{33}$$

where p_n, ρ_n, and ϑ_n are respectively the effective twist pitch length, the effective resistivity, and the average void fraction of cabling stage n. The effective resistivity ρ_n refers to the contact resistance and plating resistance of the contact section, then p_n and ρ_n are calculated by following equations:

$$\begin{aligned} p_n &= p_n - \frac{r_{n-1}}{R_{n-1}} p_{n-1} \\ \rho_n &= \frac{\rho_b e_b}{\varepsilon_n R_{n-1}} + R_{contact} R_{n-1} \end{aligned}, \tag{34}$$

where p_n is the cabling twist pitch for full back twist, ε_n is the contact area ratio, R_n and r_n are the outer and the twist radius in stage n, respectively, which were calculated by geometrical method [14]. and r_0 and R_0 were the filamentary zone radius and round wire radius, respectively. The contact resistance $R_{contact}$ of inter-strands and inter-sub-cables is defined with unit of Ω, where ρ_b and e_b are the material resistivity and the thickness of the plating, respectively. ε_n is the contact area ratio of each stage sub-cables, the contact area ratio and the radius of sub-cable have following relations:

$$\varepsilon_n = \frac{R_{n-1}}{R_n} \varepsilon_{n-1}. \tag{35}$$

This formula is accurate in the range of the void fraction between 28 and 40%, and it can be known that the ratio of contact area increases as the radius of the twisted cable decreases. In this book, Dr. Rong introduces a method to calculate the contact area ratio by the geometrical method.

The micrograph cross section and simplified diagram of the NbTi superconducting strands are shown in **Figure 7** [15], the strand cross section is simplified into three parts such as the copper core zone, superconducting filamentary zone, and copper shell zone, whose radii are measured by the simplified diagram, listed in **Table 1**. In
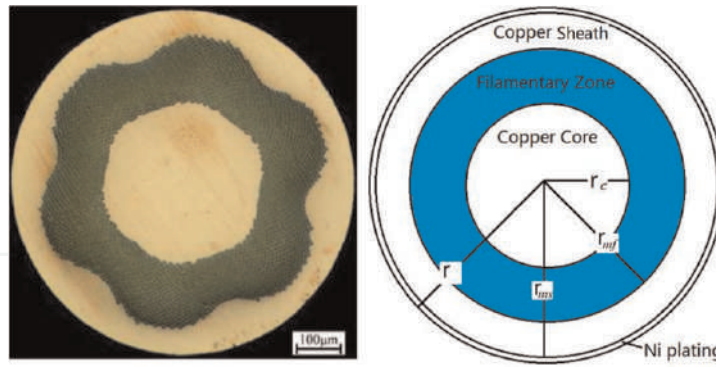
Figure 7.
The cross section and schematic layout of the superconducting strand of the ITER main busbar.

the superconducting filamentary zone of the busbar strands, there is no high resistance layer around the superconducting filaments and a high resistivity layer zone, then the radius of the filamentary shell zone equals the radius of the high resistivity layer, which all equals the radius of the filamentary zone, meaning that $r_{mf} = r_b = r_f$. Thus, the coupling losses of filamentary shell zone and high resistivity zone equals to 0, meaning that $\tau_{mf} = \tau_b = 0$, so the time constant τ_0 of the superconducting strands consists of following four contributions,

$$\tau_0 = \tau_c + \tau_f + \tau_{ms} + \tau_e, \tag{36}$$

where τ_c, τ_f, and τ_{ms} are the time constant of the copper core, filamentary zone, and the copper shell zone, respectively, and τ_e dues to eddy current. The matrix of the NbTi strands is copper.

$$
\begin{aligned}
\tau_c &= \frac{\mu_0}{2\rho_{Cu}}\left(\frac{p}{2\pi}\right)^2 \frac{r_c^2}{r_{ms}^2} \\[6pt]
\tau_f &= \frac{\mu_0}{2\rho_{tf}}\left(\frac{p}{2\pi}\right)^2 \frac{r_f^2 - r_c^2}{r_{ms}^2} \\[6pt]
\tau_{ms} &= \frac{\mu_0}{2\rho_{Cu}}\left(\frac{p}{2\pi}\right)^2 \frac{r_f^2}{r_{ms}^2}\frac{r_{ms}^2 - r_f^2}{r_{ms}^2 + r_f^2} \\[6pt]
\tau_e &= \frac{\mu_0}{8\rho_{Cu}}\left(r_c^2 + \frac{\delta\left(r_f^4 - r_c^4\right)}{r_f^2} + \frac{r_{ms}^4 - r_f^4}{r_{ms}^2}\right)
\end{aligned}
\tag{37}
$$

Where ρ_{Cu} is the resistivity of the copper matrix of the superconducting strand, ρ_{tf} is the transverse resistivity in the filamentary zone, in which the contact resistance of filament-to-matrix R_{cmf} is $5.5 \times 10{-}15 \ \Omega m^2$ [13]; and δ is the copper ratio of the filamentary zone, which could be calculated by the following:

$$\delta = \frac{1}{1+\lambda}, \tag{38}$$

where λ is the ratio of the superconductor to the matrix in the superconducting filament zone.

Zone	Core	Filamentary	Shell	Due to eddy	Sum strand
$\tau(ms)$	6.94	38.72	3.62	1.65×10^{-4}	49.08

Table 2.
The coupling time constant of the superconducting strand.

The coupling time constant of the superconducting strand of the TF main busbar of ITER is calculated, and the total coupling time constant of the strand is 49.08 ms, as shown in **Table 2**.

The TF main busbar of ITER is wound from multiple stage sub-cables made with cooper and superconducting strands, and there is inducing current flow between adjacent strands and adjacent sub-cables, so there are coupling losses in sub-cables. All strands, both superconducting and copper strands, are Ni-plated to induce AC losses and to guarantee stable contact resistance with time. The cable pattern (strand as the first stage) of the TF-MB is (2SC + 1Cu) × 3 × 5 × (5 + C0) × (6 + C1), where C0 is 3 × 4Cu, and C1 is (1 + 6 + 12 + 18 + 24)Cu, as shown in **Figure 2**. The main busbar cable is simplified to five stages sub-cable for coupling time constant calculation, as shown in **Figure 8**, R_n and r_n are respectively the outer and the twist radius of the *nth* stage sub-cables, which carried out by a geometric method according to **Figure 8**, and r_0 is the strand filamentary area radius of the superconducting strand, while R_0 is the radius of the strand.

The effective resistivity of the sub-cables refers to the thickness and resistivity of Ni-plating and contact resistance, and the contact resistance is affected by the loading cycles. The contact resistance inter-strands and inter-sub-cables are tested in SULTAN [16–18] (the length of the simple is 0.5 m), where the Ni-plating petal has a peak contact resistance, and gradually decreases to 150 nΩ at cycle 30,000, and does not change much after 30,000 cycles. Despite the difference in applied load and conductor type, all measured conductors show inter-petal contact resistance around 150 nΩ after 30,000 loading cycles. And the inter-strands contact resistance is around 75 nΩ after 30,000 loading cycles. In the ITER feeder system, the main busbar is assembled by enough loading cycles burn-in conductor, so in 15MA Plasma Current Reference Scenario, the inter-strand contact resistance of 75 nΩ and inter-petal of 150 nΩ are chosen during coupling time constant calculation.

The contact area ratio is the ratio between the real contact and the surface area of the sub-cables, which is a key parameter for the coupling time constant. It is known
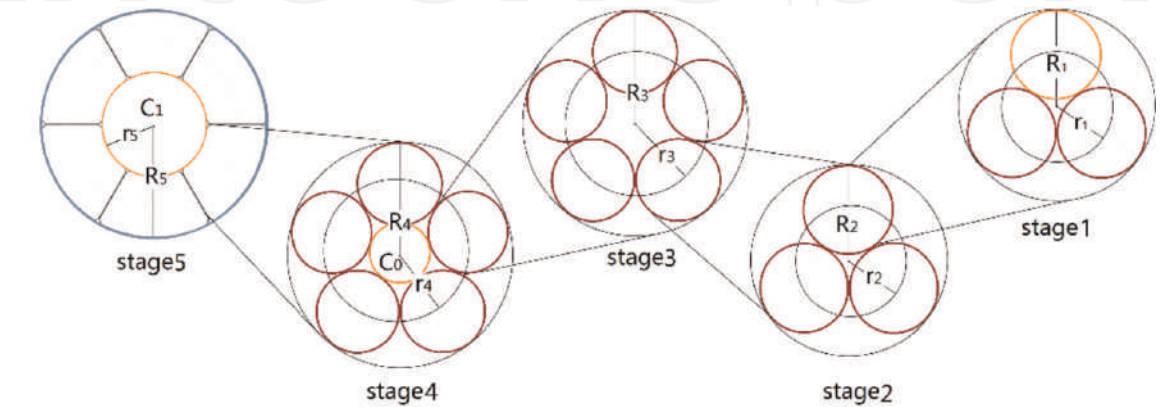

Figure 8.
The schematic view of the cabling geometry of the ITER TF main busbar.

that the contact area ratio of sub-cables could be calculated by Eq. (35), and the contact area ratio of the first sub-cable means that the contact area ratio between strands, is assumed a typical value of 20% [19]. However, contact area ratios of cables with different average void fractions are different, in the last stage sub-cable, the contact area ratio is quite low, because the pattern of the last stage sub-cable is petal structure, and there is wrap wrapped petals sometimes. In this chapter, a geometric method is introduced to estimate the contact area ratios between strands and of the last stage sub-cables, in which the contact angular thicknesses between two strands and between two sub-cables are the same. In the first stage, the contact area ratio could be estimated by the following equation:

$$\varepsilon_1 = \frac{l_{r1}}{l_{r2}}, \tag{39}$$

Where ε_1 characterizes the area of contact between two strands, l_{r1} refers to the contact line (red), and l_{r2} refers to the perimeter, meaning that the contact line (red) plus un-contact line (green), as shown in **Figure 9(a)**. In the ITER TF main busbar conductor, the first stage sub-cable consists of three green strands, and there is an indentation between contacted strands, as shown in **Figure 9(a)**.

In the bundle of the main busbar, if the cross section of the strands is standard circle, the bundle void fraction could be calculated by following equation:

$$\vartheta_{bundle} = 1 - \frac{(N_{SC} + N_{Cu})R_0^2\pi}{(R_5^2 - R_5^2)\pi}, \tag{40}$$

In the TF main busbar conductor, the calculated bundle void fraction with standard circle strand equals 44.55%, which is higher than the tested bundle void fraction of 38.78%, meaning that the strands are extruded to deformation, and it could be confirmed by the indentation in the untwisted strands. The indentation in the strand and the helium flow channel between adjacent strands are assumed same, then the
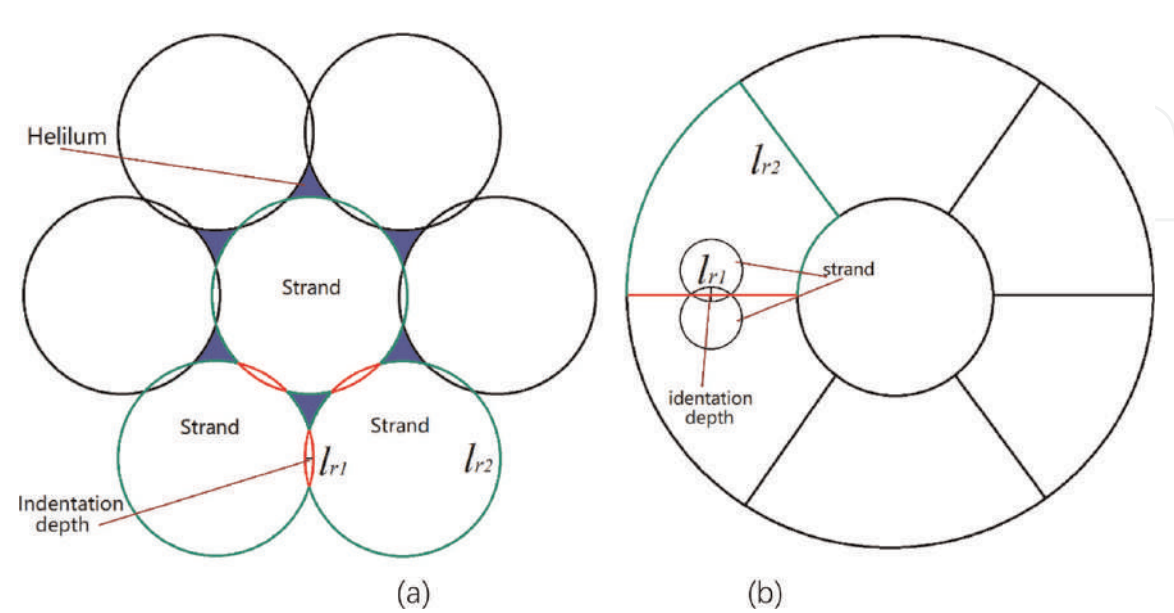

Figure 9.
The diagram of contact between Bi-2212 round wires (a), the diagram of contact between last stage sub-cables (petals) (b) for contact area ratio calculation.

indentation depth could be calculated by the bundle void fraction induction, as shown in **Figure 9(a)**, the blue area is the bundle helium flow channel.

In the last stage sub-cable of the TF main busbar conductor, the conductor is cabled by six petals, as shown in **Figure 9(b)**. The strands between two petals contact just like the red line of **Figure 9(b)**, then the contact area ratio between two petals, could be evaluated by Eq. (39). In which, l_{r1} refers to the contact line (red), and l_{r2} refers to the contact line (red) plus the un-contact line (green).

In 15MA plasma current reference scenario, the coupling time constant of the TF main busbar is carried out by Eq. (32), the coupling time constant after 30,000 loading cycles is calculated as 253.76 ms. The time constant of the cable is tested in SUTAN, $n\tau$ are about 160 ms after 10 cycles and 279 ms after 1000 cycles, respectively [20].

There are AC losses in the superconducting conductor, and also AC losses present in the superconducting joint, farther more, there is joule heating in the joint caused by the joint resistance. The AC losses and joule heating of the joints could cause a temperature rise in the main busbar, which reduces the temperature margin. In the next section, a development of petals overlap joint will be discussed in detail, the joint has lower resistance and AC losses, and small volume, which cause a lower temperature rise comparing with twin-box joint. And other improvements about the petals overlap joint are given, such as better coolant channels, more isotropous insulator stress around the joint.

3. The petal overlap superconducting joint for ITER TF main busbar

Typically, the superconducting busbar of the TOKAMAK feeder system is divided into several segments, which are connected by superconducting joints. In this section, a petal overlap superconducting joint for ITER TF main busbar will be discussed.

3.1 The design of the petal overlap superconducting joint

The current and coolant of the superconducting magnet are supplied by the Feeder, and for the purpose of assembly and mechanical redundancy, the feeder is divided into Coil-Terminal-Box (CTB), S-Bend-Box (SBB), Cryostat Feed-through (CFT), and In-Cryostat Feeder (ICF) [9, 21–23]. The following are the design requirements from ITER organization:

- The resistance of the joint should be lower than 2 nΩ at the condition of 4.5 K temperature, none background field, and carrying 68 kA current [24].

- After temperature rise caused by AC losses and resistance, the main busbar should have a temperature margin above 2.0 K [25, 26].

- In the joint, each strand of the cable should have ohmic contact with the copper sole, thus the copper sole of the joint should be longer than the twist pitches of the sub-cable contacted with it.

For lower resistance, smaller volume, and more uniform tension insulators joints, Dr. Rong developed a petal overlap joint design, as shown in **Figure 10**.
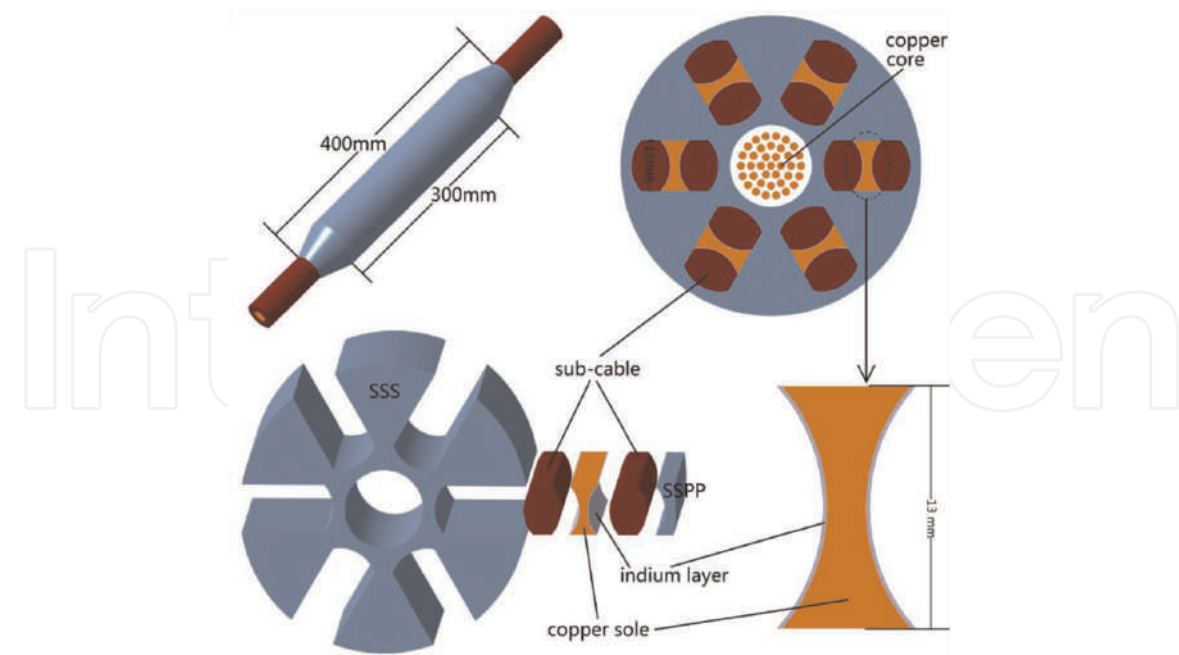
Figure 10.
The petal overlaps joint.

The assembly procedure of the petal overlap joint is set referring to twin-box joint:

a. Untwist the cable, get six petals and one copper core with length of 600 mm, and remove the nickel on the outer layer strands of petals by reverse electroplating process, but the inner layer remained.

b. Plate a 4 μm thickness silver plating-layer on sub-cables and copper soles, coat about 0.2 mm thickness pure indium layer on both sides of copper soles, and clean the surface of the indium layer.

c. Put one copper core through the central hole of stainless-steel support (SSS), and connect it with another copper core by copper strand welded.

d. Put six petals of one busbar, six copper soles, six petals of another busbar and stainless-steel pressure plates (SSPP) into the six grooves of SSS in turn, the length of SSS and copper is 300 mm.

e. Exert about 100 tons of pressure at room temperature (referring to twin-box assembly) to the SSPP till about 14 days later, and SSS and SSPPs are welded together.

In the petal overlap joint, the superfluid helium coolant flows through the bundle void of petals and core hole without external cooling pipes. It is known that cylinder makes insulators tension more uniform. In the complex electric-magnetic field, there will be AC losses and joule heating in the superconducting joint, which are important parameters, will be discussed in detail in the next subsection.

3.2 The joule heating and AC losses of petal overlap joint

Just like twin-box joint, in the resistance calculation model of petals overlap joint, **Figure 11(a)** shows the current flows direction, the current is carried by superconducting filaments only in the cable, while the copper matrix, indium layers, silver layers, and copper soles carry the current together in the joint, thus the joint resistance consists of copper matrix resistances, indium layer resistances, silver layer resistances, copper sole resistances, and contact resistances. The filament-to-matrix contact resistances could be estimated by the comparison of simulation with experimental results in the Twente Press Experiment [27–30]. As shown in **Figure 11(b)**, in the joint resistance calculation model, the two cables were equivalent to a homogeneous superconductor plus an equivalent resistance layer, the equivalent resistance layer represented the resistance of filament-to-matrix and copper matrix. Then the joint resistance consists of two equivalent layer resistances, two copper sole resistances, three indium layer resistances, and six silver layer resistances.

In the resistance simulation, because of low enough resistivity of 3.6×10^{-3} nΩm at 4.5 K temperature and thin enough thickness of 4 μm, the resistance contribution of silver is neglected [31], the superconductor resistivity is set at a low enough value of 1.0×10^{-6} nΩm to simulate zero resistance, as listed in **Table 3**. According to the experiment of joint assembly, the thickness of indium layer is set 0.2 mm, whose electrical conductivity is 7.46×10^{10} S/m at temperature of 4.5 K, according to Indium Corporation, [32, 33], as listed in **Table 3**. The current flows from cable to cooper sole through the outer layer strands, and the strand diameter 0.73 mm, then, the thickness of the equivalent resistance layer is set 0.365 mm, and the resistivity of the resistance layer is set equaling effective filament resistivity [27].

The twin-box resistance calculation model is used to verify the accuracy of the equivalent of the model, as shown in **Figure 12(a)**, in the joint resistance calculation model, a 68 kA DC load is applied on one busbar cable, and grounded another cable, the calculation resistance of the twin-box joint is 0.201 nΩ, while the test resistance was 0.2 nΩ carried out in ASIPP. Thus, the joint resistance calculation model was acceptable. In the petal overlap joint resistance calculation model, the petal overlap
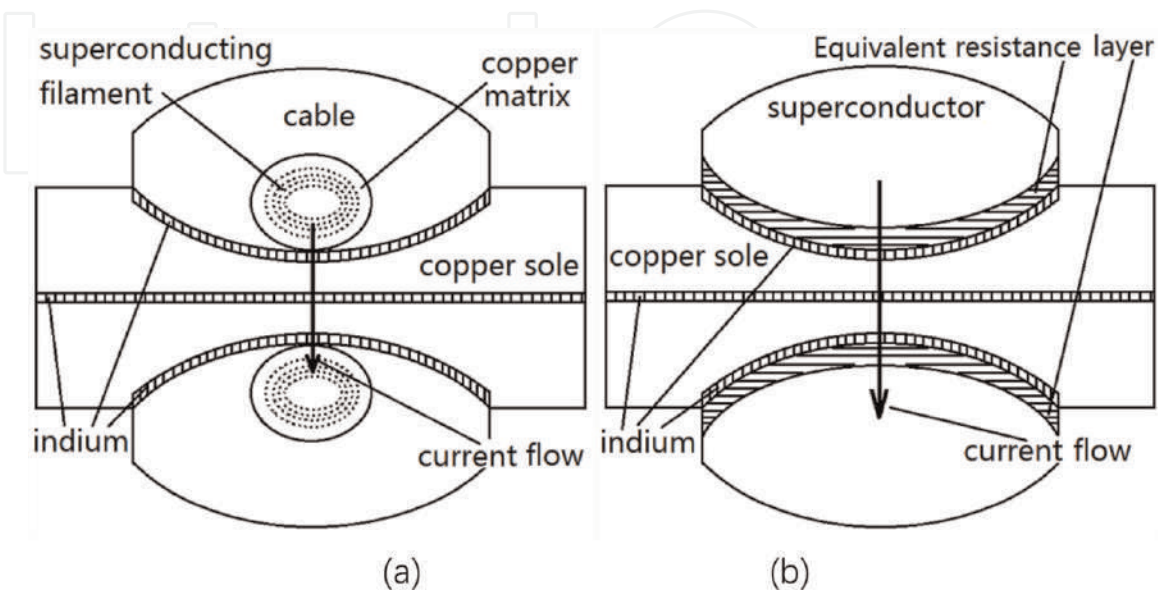

(a)   (b)

Figure 11.
The cross section and current flow diagrams of (a) realistic joint and (b) resistance calculation model.

material	Resistivity(nΩm)	Electrical conductivity (S/m)
Silver	3.6×10^{-3}	2.78×10^{11}
Superconductor	1.0×10^{-6}	1.0×10^{15}
Equivalent resistance layer	1.7	5.88×10^8
Copper	0.18	5.56×10^9
Indium	1.34×10^{-2}	7.46×10^{10}

Table 3.
The resistivity of the joint calculation model.
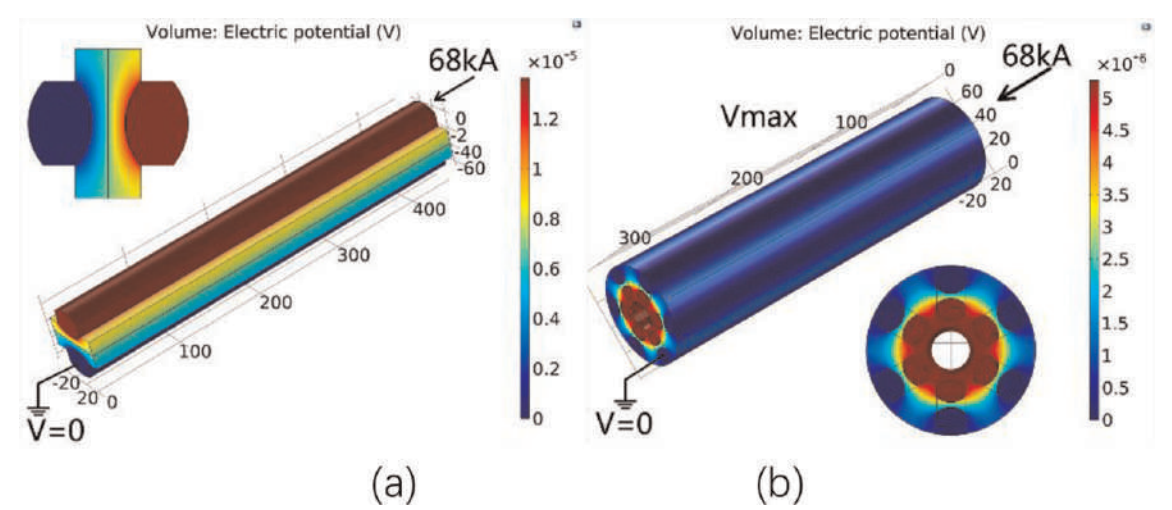
Figure 12.
The electric potential distribution in (a) twin-box joint and (b) petal overlap joint used for joint resistance calculation.

joint model was applied a 68 kA DC load on the petals of one busbar cable, and grounded the petals of another cable, as shown in **Figure 12(b)**. The petal overlap joint resistance was calculated at 7.76×10^{-2} nΩ.

In 15 MA reference scenario, the significant field variation only presents at the location near the terminal joint, therefore the joint AC losses are only significant in the terminal joints. AC losses of the joint were calculated with the following method [34]:

$$B + \tau \frac{dB}{dt} = B_a \quad P_{AC-joint} = \frac{n\tau}{\mu_0}\left(\frac{dB}{dt}\right)^2 V, \tag{41}$$

Where B_a stands for the external magnetic field, whose direction is related to the studied contribution, while B stands for the local field. The demagnetization factor n is 1 for a slab, while 2 for a round. $P_{AC-joint}$ stands for AC losses of the twin-box joint, V is the effective shielded volume, and τ stands for the time constant of induced currents.

During the AC losses of the petal overlap joint calculation, the petal overlap joint is equivalent to six twin-box joints, while the AC losses of SSS and SSPP are neglected because of its high resistivity. **Figure 13** shows the geometrical simplification of one
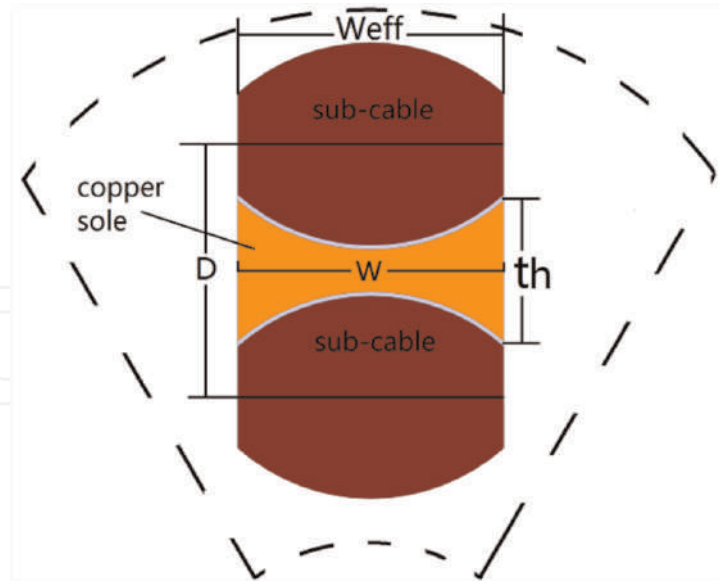
Figure 13.
The geometrical simplification of twin-box joint simplified by petal overlap joint.

twin-box joint simplified from petal overlap joint. Then the AC losses calculation method of twin-box could be used to calculate the AC losses of petal overlap joint:

a. The field normal to the copper sole causes coupling loss and eddy current loss, whose coupling time constant τ_{trans} carried out by the following [35]:

$$\tau_{trans} = \frac{\mu_0 W^2}{12 \rho_{copper}}, \tag{42}$$

As shown in **Figure 13**, and listed in **Table 4**, W stands for the width of the copper sole, whose resistivity ρ_{copper} is listed in **Table 3**. The effective volume (V_{trans}) equals the volume of the copper sole plus cables.

b. The field tangent to the copper sole and normal to the cables causes coupling loss and eddy current, whose coupling time constant τ_{cond} is carried out by the following [35]:

$$\tau_{cond} = \frac{L_1 - L_2 - 2M}{R_{m1} - R_{m2}}, \tag{43}$$

where L_1, L_2 stand for self-inductance of two cables in the joint, while M stands for the mutual-inductance of the two cables. R_{m1} and R_{m2} stand for equivalent resistance of the two cables [35]. The effective volume (V_{cond}) equals the volume of half-cables.

c. The field produces the inter-cable current, which causes loss referring to the copper sole and normal conductor of the cables. The coupling time constant τ_{joint} could be carried out by the following [35]:

$$\tau_{joint} = \frac{\mu_0 L D}{12 W_{eff} R_{joint}}, \tag{44}$$

Where L, W_{eff}, and D, stand for the joint length, the effective width of sub-cables of petal overlap joint, and the distance of two sub-cables in a petal overlap joint respectively, listed in **Table 4**. R_{joint} stands for the resistance of one simplified twin-box joint. The effective volume (V_{joint}) is carried out by the following:

$$V_{joint} = L \bullet W_{eff} D. \tag{45}$$

The AC losses of the three contributions are carried out by Eq. (47) with field variations referring to IDM_45SA69 of ITER organization, as listed in **Table 5**. The AC loss of one twin-box joint simplified from the petal overlap joint is about 0.197 W, as listed in **Table 5**. Then the AC loss of total petal overlap joint is 1.182 W.

Ohmic heating produced by the joint resistance and transport current was calculated by the following equation:

$$P_{ohmic} = R_{joint} I_{op}^2, \tag{46}$$

Geometrical parameters	Units	One simplified twin-box joint in petal overlap joint
W_{eff}	mm	13
W	mm	13
th	mm	7.2
D	mm	12
L	mm	300
V_{trans}	mm^3	0.076
V_{cond}	mm^3	0.061
V_{joint}	mm^3	0.047

Table 4.
The geometrical parameters of petal overlap joint.

Calculation losses	Units	One simplified twin-box joint in petal overlap joint
τ_{trans}	s	0.098
τ_{cond}	s	0.2
τ_{joint}	s	20.49
P_{trans}[a]	nW	7.76×10^{-3}
P_{cond}[b]	W	0.18
P_{joint}[c]	W	0.017
$P_{AC-joint}$	W	1.182
P_{ohmic}[d]	W	0.36
P_{total}	W	1.542

Table 5.
The losses of and petal overlap joint.

where R_{joint} is joint resistance, and I_{op} is the transport current. The Ohmic heating is calculated at 0.36 W produced by petal overlap joint, as listed in **Table 5**.

The AC losses and joule heating could cause a temperature rise in the main busbar, which could reduce the temperature margin. Then, the temperature rise caused by petals overlap superconducting joints will be analyzed carefully in the next subsection.

3.3 The temperature rise caused by the petal overlap joint

According to ITER requirements, the design temperature margin of the main busbar should be above 2.5 K. The temperature margin (ΔT) reflects the ability of removing heat of surrounding helium before the quench of the superconducting strands [36, 37].

The THEA code is used to simulate the main busbar with petal overlap joints in 15 MA scenario. During operation, there are AC losses of busbar and joints, joule heating of the joints, heat exchange in the joints, and the heat load from supports and HTS (high-temperature superconductor), which cause a temperature rise, and are taken account into the THEA model. Busbar cable AC losses (including coupling and hysteresis losses) have been calculated by M. Nannini (ITER organization IDM_45SA69), whose maximum value is about 1.33 W/m. In the THEA model, busbar cable AC losses are assumed constant along the busbar, which equals the maximum value. There are five joints in each main busbar at the locations of 0 m, 6.5 m, 12.9 m, 25.3 m, and 36 m, respectively.

As shown in **Figure 14(a)**, there are five temperature rises in the location of the joints, the temperature increases along the main cable same direction with the helium flowing, and the maximum temperature in the busbar cable with petal overlap joints was 5.5 K, which occurred at the location of the fifth joint, this maximum temperature was added by HTS current leader heating mainly.

The current sharing temperature (Tcs) refers to the able pattern and the operation current, and its distributions of respective busbar did not change with time, as shown in **Figure 14(b)**, the current sharing temperatures were almost
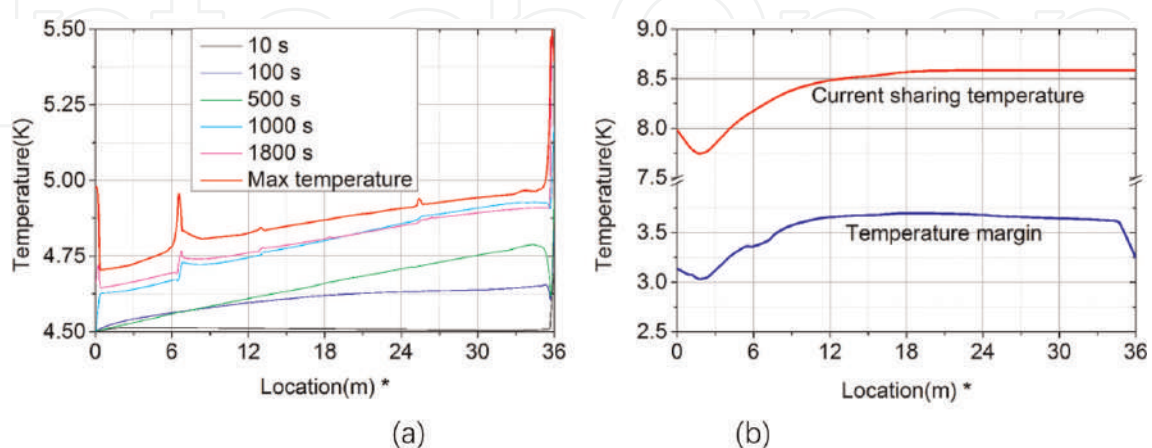

Figure 14.
(a) The temperature distribution of busbar with petal overlap joints, and (b) current sharing temperature and temperature margin distributions of busbar with petal overlap joints (*the coordinate of "location(m)" in the figures is the location of main busbar, and 0 m is located in the end of busbar near the magnet).

impervious to joint heating. The temperature margin was calculated by the following equation:

$$\Delta T = T_{cs} - T_{max}, \tag{47}$$

where T_{max} is the maximum temperature at each location (as shown in **Figure 14(b)** thick red lines) of the busbar cable. The lowest temperature margin of cable with petal overlap joints was 2.85 K, which reached ITER requirements.

The effects of joints to the main busbar are analyzed carefully; however, there are disturbances in the main busbar conductor, which could cause a nonrecoverable quench. In the next section, the stability and quench behavior of the main busbar will be discussed in detail.

4. Stability and quench behavior analysis of the ITER TF main busbar

In the ITER TF main busbar, there are static and AC losses in the superconducting conductor, such as heat exchange in joint, joule heating in joint, AC losses in joint, control losses, radiation from 80 K cooling, vacuum barrier conduction, external support and peak AC losses in conductor, which could cause a temperature rise in the conductor. The temperature rise could reduce the temperature margin of the superconducting conductor, and the temperature margin should be set large enough to guarantee the stability of the conductor after covering the static and AC losses. During superconducting magnet operation, the superconducting conductor is considered to quench, once the operation temperature exceeds the current sharing temperature.

During superconducting magnets operation, the mechanical displacement, increased local stress and local shear force could cause the local thermal deposition in the superconductor, which could cause an unrecovery quench in the superconducting conductor. The smallest energy that causes an unrecovery quench is called minimum quench energy (MQE).

After quench, the current is carried by the normal conductor, and the temperature rises, then the current is cut down, and then the temperature of the conductor rises unceasingly because of the residual energy left in the magnet. The maximum temperature is called hotspot temperature, which refers to the ratio of superconductor and normal conductor.

In this section, the temperature margin, minimum quench energy, and hotspot temperature of the ITER TF main busbar will be discussed in detail.

4.1 The temperature margin of the ITER TF main busbar

The TF main busbar has a copper core (C0), as shown in **Figure 15**. which is cooled internally with forced flow supercritical helium at an inlet temperature of 4.5 K and inlet pressure of 6.0 bar, and the operation current is 68 kA [2, 9, 10, 25], as listed in **Table 1**, the bundle helium flows in the bundle void, while hole helium flows in the rope void, shown in **Figure 15**.

The temperature margin provides a margin against uncertainties in the strand performance (e.g., critical current, temperature) and a capacity for heat absorption in
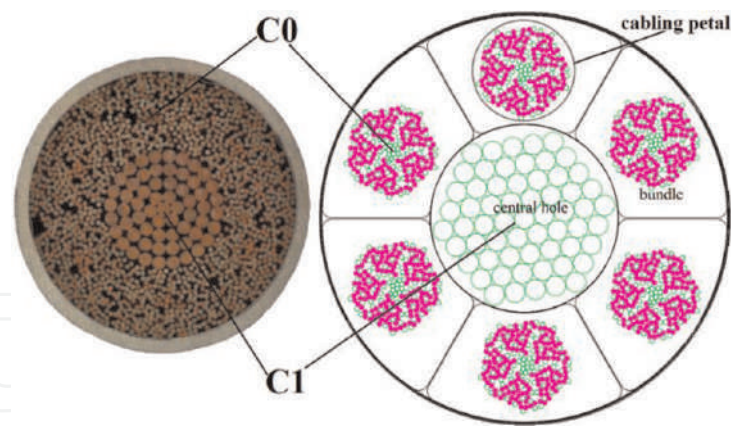
Figure 15.
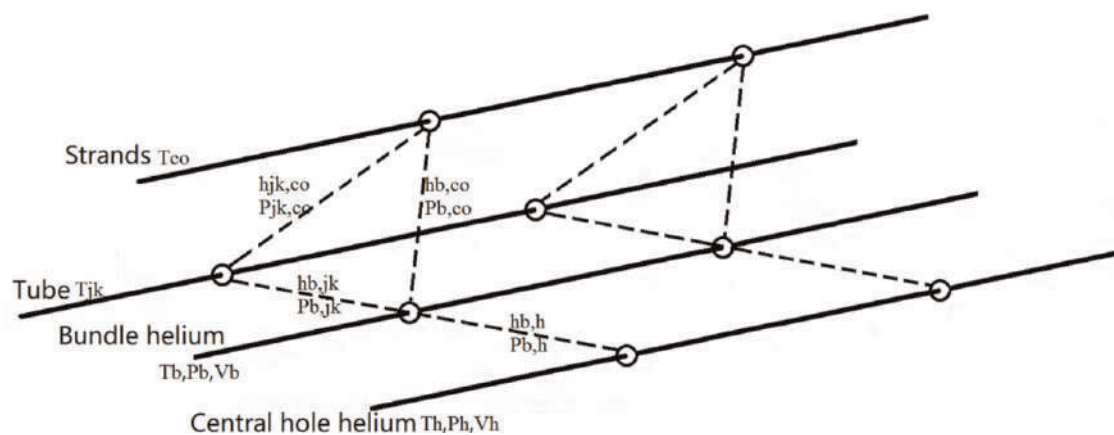*Schematic of the main busbar cross-sectional layout.*

Figure 16.
Schematic of the one-dimensional finite element model of TF main busbar.

the surrounding helium before the strands quench [36, 37], the temperature margin could be carried out by Eq. (47).

The temperature behavior of the busbar during 15 MA scenario is analyzed by one-dimensional finite element numerical simulation. The following simplifying assumptions of Gandalf are significant for this study, as shown in **Figure 16**:

a. the current is uniformly distributed among the strands;

b. the disturbance is applied uniformly in the conductor cross section;

c. all copper in the cable is included as a stabilizer;

d. the two-fluid model (forced flow helium flowing in the hole and the bundle) is used in this analysis.

As shown in **Figure 16**, the coupling of the model is given by heating exchanging between the four sub-one-dimensional models, and the liquid helium fluid abides by the law of conservation of mass (the continuity equation), the law of conservation of energy (Bernoulli's equation), and the law of conservation of momentum (momentum equation) [38–40]:

$$\frac{\partial V_b}{\partial t} + V_b \frac{\partial V_b}{\partial x} + \frac{1}{\rho}\frac{\partial P}{\partial x} = -2f_b \frac{V_b|V_b|}{D_{hb}}$$

$$\frac{\partial V_h}{\partial t} + V_h \frac{\partial V_h}{\partial x} + \frac{1}{\rho}\frac{\partial P}{\partial x} = -2f_h \frac{V_h|V_h|}{D_{hh}}$$

$$\frac{\partial P}{\partial t} + a_b\rho c^2 \frac{\partial V_b}{\partial x} + a_h\rho c^2 \frac{\partial V_h}{\partial x} + V\frac{\partial P}{\partial x} = \Phi(a_b V_b F_b + a_h V_h F_h) + \frac{\Phi Q_{He}}{A_{He}}$$

$$\frac{\partial T_{He}}{\partial t} + a_b\Phi T_{He}\frac{\partial V_b}{\partial x} + a_h\Phi T_{He}\frac{\partial V_h}{\partial x} + V\frac{\partial T_{He}}{\partial x} = \frac{a_b V_b F_b + a_h V_h F_h}{C_v} + \frac{Q_{He}}{A_{He}\rho C_v}$$

$$AC\frac{\partial T_{co}}{\partial t} - A\frac{\partial}{\partial x}\left(k\frac{\partial T_{co}}{\partial x}\right) = -Q_{He,co} + Q_{joule} + Q_{ext} - Q_{co,jk}$$

$$A_{jk}C_{jk}\frac{\partial T_{jk}}{\partial t} - A\frac{\partial}{\partial x}\left(k_{jk}\frac{\partial T_{jk}}{\partial x}\right) = -Q_{He,jk} + Q_{joule,jk} + Q_{ext,jk} - Q_{co,jk}$$

(48)

Where V_b and V_h are the flow velocity of bundle and central helium respectively, D_{hb} is the hydraulic diameter of the bundle helium, P is the pressure of helium, c is the acoustic velocity of super-critical helium, Φ is the Grüneisen parameter of helium, ρ is the density of helium, C_v is the specific heat at constant volume of helium, A, A_{jk}, A_b, A_h, and A_{He} are the cross-sectional areas of conductor, jacket, bundle helium, central hole helium, and the total helium, respectively, and V, a_b, a_h, F_b, and F_h could be given by the following:

$$V = a_b V_b + a_h V_h$$

$$a_b = \frac{A_b}{A_{He}} \quad a_h = \frac{A_h}{A_{He}}$$

$$F_b = 2f_b \frac{V_b|V_b|}{D_{hb}} \quad F_h = 2f_h \frac{V_h|V_h|}{D_{hh}}$$

(49)

Where f_b and f_b are the coefficients of friction of bundle and central helium, respectively.

The equation could be solved by the finite element method, time is dispersed by the numerical approach method, while the spatial is dispersed by the Galerkin method, and the upwind is used to simulate the flow direction of helium. In this study, the Gandalf code is used to study the behavior of the TF main busbar in 15MA plasma current reference scenario.

The temperature margin is simulated by THEA code. In the 15 MA reference scenario, there AC losses, joule heating, and other losses in the main busbar, which could disturb the stability of the busbar, and the superconducting cable must be able to absorb them without causing a quench. In the THEA model, all losses are applied directly into the conductor as the external linear heating input, which is a square wave in space and time, which is assumed uniform along the conductor, as shown in **Table 6**. In the 15 MA scenario, AC losses are estimated and tested in SULTAN [15, 20, 41], which is 1.38 W/m in the plasma building phase (0–200 s), and is neglected after 200 s. Then the external heating input of the model is shown in **Figure 17**, and the following conditions are used for the model [2, 9, 10, 25]:

Parameters	Value	Units
Heat exchange in joint	9.3	W
Joule heating in joints	47	W
AC losses in joint	1.4	W
Control losses	3.3	W/m
Radiation from 80 K	3.3	W/m
Vacuum barrier conduction	2.73	W
External support	7.6	W
Peak AC loss in cable	1.38	W/m

Table 6.
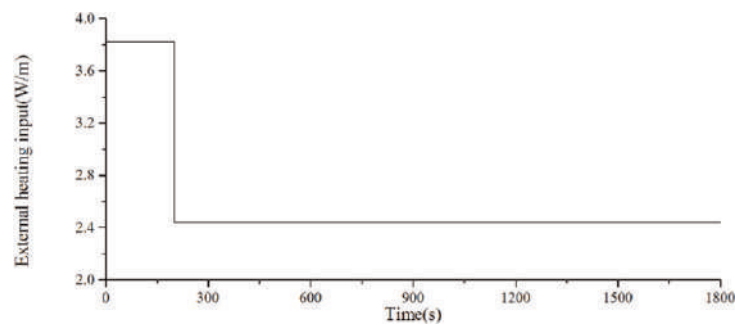*Summary of the static and AC losses for the main busbar in 15 MA scenario.*

Figure 17.
External heating input of Gandalf model during 15 MA scenario.

a. The cable length is set 30 m for the worst case and without jumpers, the inlet temperature is 4.5 K, inlet pressure is 6.0 bar, and the mass flow of helium is 10.5 g/s.

b. The time step is set as 1 s, and the maximum mesh sizes is 0.1 m for a stable purpose.

c. The cross-sectional areas of bundle helium and the hole helium are 417.8 mm^2 and 47.9 mm^2 repectively.
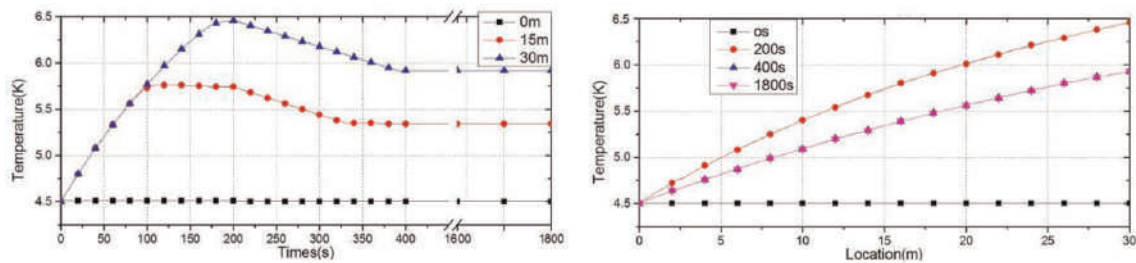

Figure 18.
Temperature behavior of the TF main busbar conductor in 15 MA reference scenario.
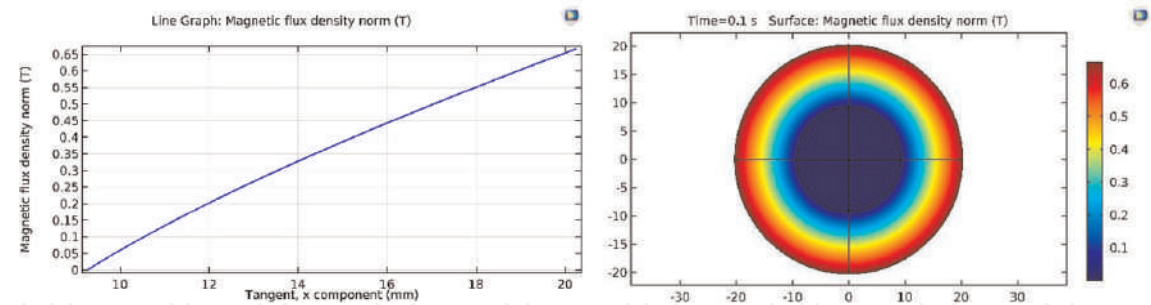
Figure 19.
Distribution of self-field in the TF main busbar cross section.

    d. The external heat flux input (all losses included) is uniform at 3.82 W/m from 0 to 200 s, and 2.44 W/m (ac losses excluded) for the remaining times.

According to the model, in the worst case, the maximum temperature is 6.45 K at the time of 200 s and the location of 30 m in the 15 MA scenario, as shown in **Figure 18**.

Temperature rise could cause a current sharing in the matrix, then there is electric field in the superconducting cable. In the engineering application, a parameter named the current sharing temperature is defined, the current sharing temperature equals the temperature, which causes an electric field value of 10 μV/m. In the 15 MA scenario with 3.0 T field, 4.5 K temperature and 68 kA operation current, the current sharing temperature of the main busbar have been carried out by Gandalf code, which equals 7.62 K. In the Gandalf model, the magnetic field distribution in the cross section of the cable is assumed uniform; however, the field is not uniform in the cross section of the cable actually, then the current sharing temperature should be estimated further exactly.

In 15 MA scenario, the self-field distribution in the main busbar cross section is simulated by the finite element method in the COMSOL model, which is not uniform, as shown in **Figure 18**.

In this study, the current sharing temperature is estimated by E-J characteristic. As shown in **Figure 19**, the self-field distribution is axis-symmetrical, then the bundle zone is divided into 220 annuluses, the difference between two adjacent annuluses is 0.05 mm. Thus, the cross-sectional area of the *ith* annulus is:

$$A_{sci} = \frac{A_{sc}}{\pi \left(r_{out}^2 - r^2\right)} \pi \left((x_i + dx)^2 - x_i^2\right). \tag{50}$$

Then the E-J characteristic could be turned into the following:

$$E_{av} = \frac{E_c}{A_{sc}} \sum_i^N A_{sci} \left(\frac{J_{op}}{J_c(B_i, T)}\right)^{n(J_c)}, \tag{51}$$

where B_i is the magnetic flux density of the *ith* annulus.

The current sharing temperature of full-size main busbar sample is tested in SULTAN, the temperature is 4.22 K, the background field is 3.22 T, and the operation current is 45.5 K. the tested current sharing temperature is 6.98 K, and the current sharing temperature from Gandalf model is 7.34 K, while current sharing temperature calculated by Eq. (51) is 7.09 K. This indicates that the method is much more accurate than the simulated value by the Gandalf model.

Operation current	kA	68
Background field	T	1.89
T_{cs} Gandalf model	K	7.62
T_{cs} Computed from COMSOL model	K	7.37

Table 7.
Current sharing temperature of main busbar used in 15 MA scenario.

In 15 MA scenario, the operation current of the TF main busbar is 68 kA current, and the background field equals 1.89 T. Then the current sharing temperature of the main busbar could be carried out by solving Eq. (51), which is 7.37 K, as shown in **Table 7**.

In the 15 MA scenario, the current sharing temperature is estimated by Gandalf model, which is 7.62 K, and that is estimated by Eq. (51) at 7.37 K. Then the temperature margin is estimated by Gandalf code, which is 3.12 K, and that is estimated by Eqs. (51) and (47) at 2.87 K.

4.2 The minimum quench energy (MQE) of TF main busbar in 15 MA scenario

Transient heating disturbance may cause a quench in the superconducting cable, then for reflecting the disturbance, a parameter called minimum quench energy (MQE) is design. The MQE is defined as the minimum trial energy, which causes a nonrecoverable quench. Generally, during MQE estimation, the energy pulse is a small spatial extent (1–10 mm) and short duration (40–100 µs) applied to the conductor, which is just sufficient to initiate a quench [42, 43].

The MQE of the TF main busbar is carried out by the one-dimensional finite element method in the Gandalf model, the temperature in the cross section of the conductor is assumed uniform, then a one-dimensional equation of heat conduction of the TF main bus bar is carried out [44–46]:

$$A \frac{\partial}{\partial x}\left(k(T)\frac{\partial T}{\partial x}\right) + I_{op}^2 R(T) + Q_{ext}(x,t) - h(T)P_{wet}(T - T_{He}) - AC(T)\frac{\partial T}{\partial t} = 0, \quad (52)$$

Where $k(T)$ is the thermal conductivity of the conductor (W/(mk)), T is the temperature of the conductor (K), T_{He} is the temperature of helium (K), I_{op} is the operation current (A), $R(T)$ is effective resistance per unit length (Ω/m), A is the area of superconductor and matrix (m^2), Q_{ext} is the external thermal deposition (W/m), $h(T)$ is the thermal conductivity from conductor to helium (W/(m^{2}K)), P_{wet} is the wet perimeter of the conductor, $C(T)$ is the specific heat per unit volume (J/(m^{3}K)), and t is the time.

In this study, the heating pulse is the linear input applied in the conductor, which have spatial extents of 1, 3, 6, 8, and 10 mm and durations of 40, 60, 80, and 100 µs. The MQE of the main busbar is estimated by Gandalf model, and the following shows the input parameters of the model:

a. The initial external heating is applied in the middle of the model, and the time extent is from 0 to heating pulse duration [45], as shown in **Figure 20**.

a. The time step is set as 10^{-6}–10^{-2} s, and the mesh size in the heating pulse region is set as 0.01 mm to keep a stable numerical analysis.
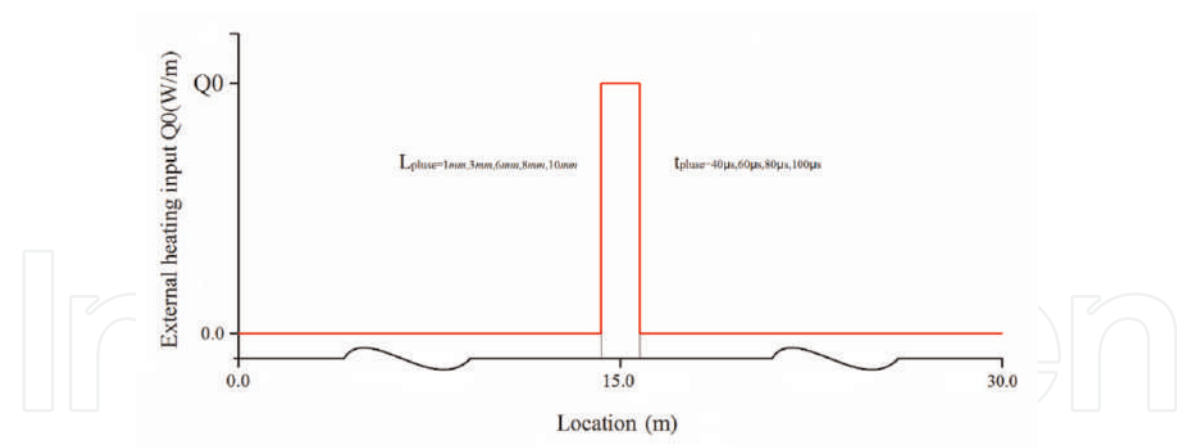
Figure 20.
External heating pulse input Q_ext in the Gandalf model.

Heat energy (J)	Heat flux (MW/m)	Recovery time (ms)
1.43	35.8	69.0
1.44	36.0	76.0
1.46	36.4	Never recovery
1.47	36.8	Never recovery

Table 8.
MQE simulated by Gandalf model with heating pulse input region length of 1.0 mm and duration of 40 μs.

b. The total delay time equals the detective time plus the delay time of the main busbar quench protection system, which equals 3.0 s, while the discharge time constant equals 11.0 s.

In the condition of heating input spatial extent of 1.0 mm and duration of 40 μs, the different heating pulse input value causes different quench behavior, as listed in **Table 8**. The MQE of the TF main busbar is set as the heating input value as following, which is 1.46 J:

$$\frac{MQE - Q_{recovery}}{MQE} < 1\%,$$

Where $Q_{recovery}$ cause a recoverable quench, and MQE causes a nonrecoverable quench.

During the MQE heating input, an instantaneous propagation quench presents, which gives a normal length L_{nor} of 26 cm. Shortly after the end of the heating pulse duration of 40 μs, the heating pulse becomes 0, the quench propagation stops, and the quench began recovery due to helium coolant heating removing. However, the normal length just becomes smaller but not vanish ($L_{nor} = 10.3cm$ at t = 20 ms), and there is joule heating produced in the normal cable. At this time, the recovery is only partial, and the quench will propagate unceasingly, because heating production is higher than heating removing. At the time of 23 ms, the normal length L_{nor} shrinks again, and at the time of 103 ms, the joule heating beats the enhanced cooling, and drives the conductor toward an irreversible quench, as shown in **Figure 21** red solid lines.
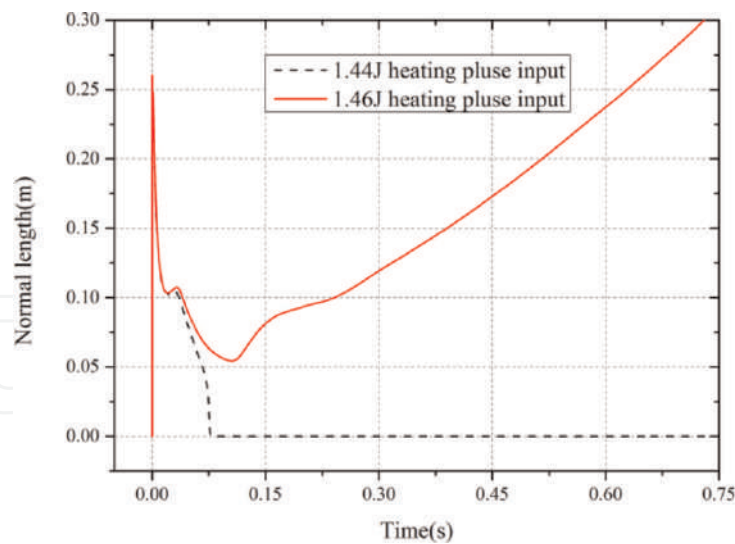
Figure 21.
Normal length in the case of quench triggered by 1.46 and 1.44 J heating pulse input.
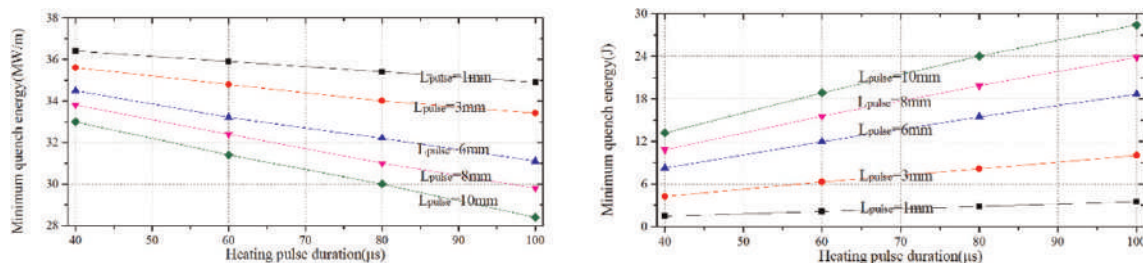

Figure 22.
MQE of the TF main busbars with heating pulse input spatial extents of 1, 3, 6, 8, and 10 mm and durations of 40, 60, 80, and 100 μs.

During the 1.44 J heating input, the quench propagation behavior is the same with the MQE heating input till the time of 33 ms; however, at this time the enhanced helium cooling is enough to drive a recovery in a few milliseconds, and then the full recovery is got at the time of about 76 ms, as shown in **Figure 21** dash lines.

The MQEs of the main busbar with different heating input spatial extents and durations are carried out by the Gandalf model, and **Figure 22** shows the MQEs of the main busbar with the heating input spatial the of 1, 3, 6, 8, and 10 mm and durations of 40, 60, 80, and 100 μs. The lower heating input per length is needed to cause a nonrecoverable quench, the larger heating pulse extents and durations.

The MQE could be affected by the operation current, because smaller current produces lower joule heating, then larger MQE is needed to cause a nonrecoverable quench. With the heat pulse spatial extent of 1.0 mm and duration of 40 μs, MQEs with different operation current are carried out by Gandalf code, as shown in **Figure 23**. It is clear that the higher operation current, the smaller MQE is needed to trigger a nonrecoverable quench.

4.3 The hotspot temperature of TF main busbar in 15 MA plasma current scenario

After an nonrecoverable quench caused by MQE occurs in the TF main busbar, the quench is detected after the delay time and during detective time, then the current of
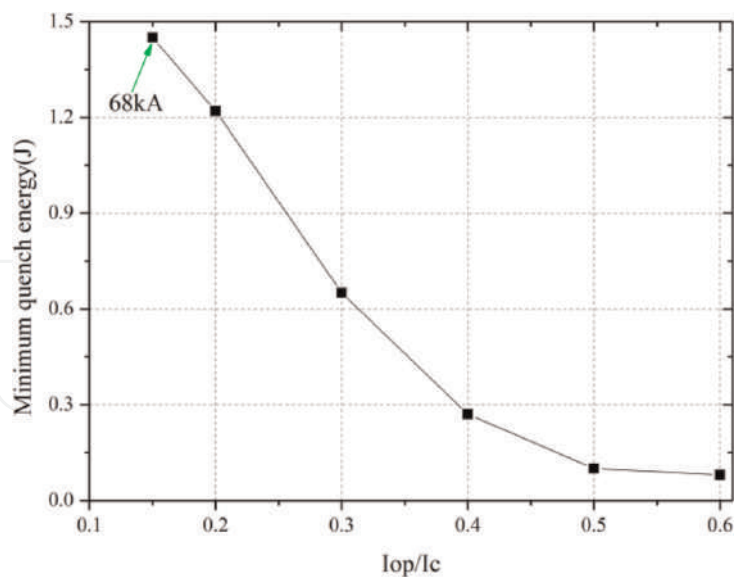
Figure 23.
MQE of the TF main busbars with different currents.

the magnet is cut down, the quench propagates along the conductor and the conductor temperature rises, till the current approaches zero gradually, in which the maximum temperature is called hotspot temperature. The hotspot temperature is one of key parameters, which refers to the copper strands ratio in the conductor, the exorbitant hotspot temperature could cause damage to the conductor. The highest hotspot temperature allowable is 150 K according to the ITER design criterion [47].

The MQE is evaluated by one-dimensional Gandalf code, the quench propagation behavior of the TF main busbar is simulated in the un-adiabatic condition. The conductor quench is initiated at the center of the conductor. The following conditions are used for the numerical simulation:

a. The inlet temperature is 4.5 K, the inlet pressure is 6.0 bar, and the mass flow is 10.5 g/s [47, 48].

b. The time step and the mesh size are set as 1–10 ms and 1 mm at the location of heating input to keep a stable numerical analysis, and 0.1 m for the rest.

c. MQE with the extent of 60 mm and duration of 0.5 ms is applied in the middle of the model.

d. The delay time equals 3 s, which is the delay time of 1 s plus the detective time of 2 s, and discharge time is 11 s [47].

In the Gandalf model, the copper strands and the copper matrix of the superconducting strands is not separated, and the Gandalf model is a two-fluid model including central hole helium and bundle helium, which is acceptable according to experimental results [49]. The MQE is applied in the middle of the model, compared with the joule heat, the MQE is low enough to be neglected during hotspot temperature estimation. The maximum temperature in the total discharge cycle is about 57.1 K with 100% extra copper, which is lower than the ITER requirement value of 150 K. In the condition of adiabatic, there is only heating conducting of conductor to remove
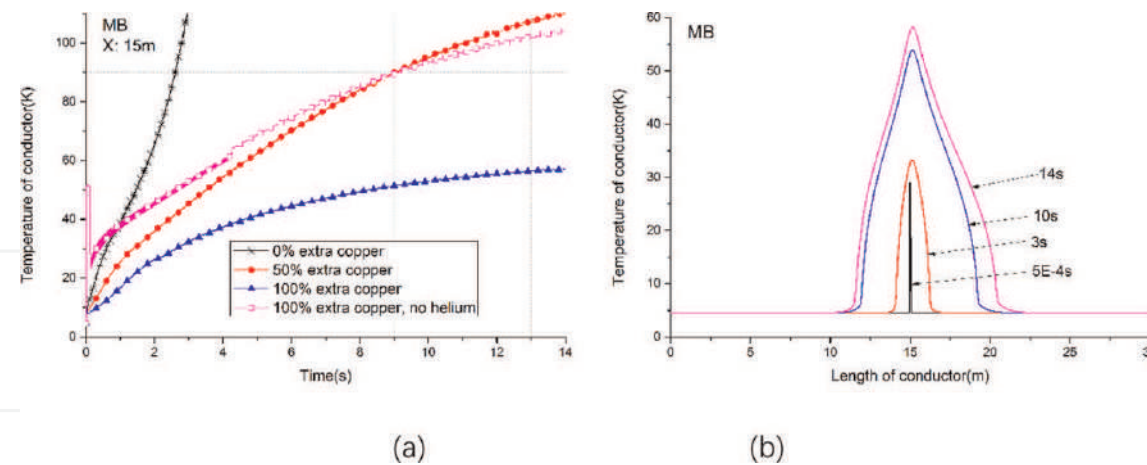
Figure 24.
(a) Temperature of conductor after quench in different extra copper content and in the case of no helium, (b) temperature distributions after quench in MB.

heating, the maximum temperature is 104 K at one discharge cycle, which is lower than the ITER requirement value of 250 K in in adiabatic condition, as shown in **Figure 24(a)**.

At the end of the heating pulse duration, the maximum temperature reaches 28 K at the middle of the model, in which the heating pulse is applied, and a nonrecoverable quench is, as shown in **Figure 24(a)**. Because of the quench, superconductor becomes normal conductor, the current is carried by copper conductor and normal superconductor jointly, which produces the joule heating, the quench propagates, and the temperature of the conductor rises gradually. The quench presents firstly at the location of the external heating pulse, and then the quench propagates along the conductor in both sides because of joule heating, the helium flows from 0 m to 30 m, so the temperature curve along the conductor presents as a dissymmetry parabola, as shown in **Figure 24(b)**.

5. Conclusions

In this chapter, AC losses calculation of ITER TF main busbar was discussed, the hysteresis loss refers to superconducting filaments, while the coupling losses refer to the pattern of the conductor, and a developed method of contact area ratio calculation is introduced. For a small impact on the main busbar form joints, a development of petal overlap joint is discussed in detail, and its AC losses and joule heating are calculated carefully; furthermore, the temperature rise caused by the joints is analyzed carefully.

The characteristics of cooling helium, inlet temperature, operation current, and external copper are some important parameters in the main busbar design, which could affect the stability and quench behavior of the main busbar. The current sharing temperature refers to the operation current, is regarded as the criterion of quench, which is calculated taking self-field account into. The minimum quench energy referring to inlet temperature and cooling helium is simulated carefully, while the hotspot temperature referring to external copper is simulated. This chapter hopes to provide some help for superconducting magnets research.

Author details

Jian Rong
School of Nuclear Science and Technology, Lanzhou University, China

*Address all correspondence to: jianrong@mail.ustc.edu.cn

IntechOpen

References

[1] Song Y, Bauer P, Bi Y, et al. Design of the ITER TF magnet feeder systems. IEEE Transactions on Applied Super-conductivity. 2010;**20**(3):1710-1713

[2] Fu, Peng, Song Y, Wu Y, et al. Recent Progress of ITER Package in ASIPP. 2018

[3] Jin F. The Theoretical and Experimental Research of Stability of CICC of HT-7U [Doctoral dissertation]. Hefei: Institute of Plasma Physics Chinese Academy of Sciences; 2002

[4] Bean CP. Magnetization of hard superconductors. Physical Review Letters. 1962;**8**(6):250

[5] Prigozhin L. The Bean model in superconductivity: Variational formulation and numerical solution. Journal of Computational Physics. 1996;**129**(1):190-200

[6] Jian R. The Electromagnetics Key Problems of TOKAMAK Superconducting Magnet and Feeder Systems [Doctoral dissertation]. Hefei: University of Science and Technology of China; 2016

[7] Bottura L. A practical fit for the critical surface of NbTi. IEEE Transactions on Applied Superconductivity. 2000;**10**(1): 1054-1057

[8] Seeber B. Handbook of Applied Superconductivity. Bristol: Institute of Physics Pub.; 1998

[9] Qin J, Wu Y, Yu M, et al. Manufacture of ITER feeder sample conductors. Fusion Engineering and Design. 2013;**88**(9–10):1461-1464

[10] Liu B, Wu Y, Qin J, et al. The performance test and analysis of ITER Main and correction Busbar conductor.

Fusion Engineering and Design. 2013;**88**: 2802-2809

[11] ITER Organization Magnet Team, ITER Magnet Feeder Busbar Design Study, ITER_D_ 2ZUR4A. 2010

[12] Miao H, Huang Y, Meinesz M, et al. Development of Bi-2212 round wires for high field magnet applications. AIP Conference Proceedings. American Institute of Physics. 2012;**1435**(1):315-324

[13] Zhou C, Miyoshi Y, Van Lanen E, et al. Inter-filament resistance, effective transverse resistivity and coupling loss in superconducting multi-filamentary NbTi and Nb3Sn strands. Superconductor Science and Technology. 2012;**25**(6): 065018

[14] Qin J, Wu Y. A 3D numerical model study for superconducting cable pattern. Fusion Engineering and Design. 2010; **85**(1):109-114

[15] Rong J, Huang X, et al. AC loss of ITER feeder Busbar in 15MA plasma current reference scenario. Journal of Fusion Energy. 2016;**35**:173-179

[16] Ilyin YA, Nijhuis A, Abbas W, et al. Effect of cyclic loading and conductor layout on contact resistance of full-size ITER PFCI conductors. IEEE Transactions on Applied Superconductivity. 2005;**15**(2):1359-1362

[17] Huang J, Ilyin Y, Wessel WAJ, et al. Contact resistance, coupling and hysteresis loss measurements of ITER poloidal field joint in parallel applied magnetic field. Superconductor Science and Technology. 2022;**35**(2):025016

[18] Yagotintsev KA, Wessel WAJ, Vostner A, et al. Overview of verification

tests on AC loss, contact resistance and mechanical properties of ITER conductors with transverse loading up to 30 000 cycles. Superconductor Science and Technology. 2019;**32**(10): 105015

[19] Ciazynski TS. A model for calculating a.c. losses in multistage superconducting cables. Cryogenics. 1996;**36**:1039-1049

[20] Yagotintsev KA et al. Superconductor science and technology accepted manuscript overview of verification tests on AC loss, contact resistance and mechanical properties of ITER conductors with transverse loading up to 30,000 cycles. Superconductor Science and Technology. 2019;**32**:10

[21] Yoshida K, Takahashi Y, Isono T, et al. Updating the design of the feeder components for the ITER magnet system. Fusion Engineering and Design. 2005;**75**:241-247

[22] Henry D, Chalifour M, Forgeas A, et al. Process flow and functional analysis of the ITER cryogenic system. AIP Conference Proceedings. American Institute of Physics. 2010;**1218**(1): 676-683

[23] Sahu AK, Gung CY, Lu K, et al. Cryogenic engineering design of the ITER superconducting magnet feeders. IEEE Transactions on Applied Superconductivity. 2012;**22**(3): 4800604-4800604

[24] Devred A, Backbier I, Bessette D, et al. Status of ITER conductor development and production. IEEE Transactions on Applied Superconductivity. 2012;**22**(3): 4804909-4804909

[25] Calvi M, Bauer P, Bessette D, et al. Design proposal for the ITER feeder

busbars. IEEE Transactions on Applied Superconductivity. 2010;**20**(3): 407-410

[26] Pong I, Vostner A, Bordini B, et al. Current sharing temperature of NbTi SULTAN samples compared to prediction using a single pinning mechanism parametrization for NbTi strand. Superconductor Science and Technology. 2012;**25**(5):054011

[27] Zhou C, Miyoshi Y, Van Lanen EPA, et al. Direct measurement of inter-filament resistance in various multi-filamentary superconducting NbTi and Nb3Sn strands. Superconductor Science and Technology. 2011;**25**(1): 015013

[28] Abbas W, Nijhuis A, Ilyin Y, et al. A fully automatic Press for Mechanical and Electrical Testing of full-size ITER conductors under transverse cyclic load. AIP Conference Proceedings. American Institute of Physics. 2004; **711**(1):51-58

[29] Rolando G. Cable-in-conduit superconductors for fusion magnets [PhD Thesis]. University of Twente; 2013

[30] Nijhuis A, ten Kate HHJ, Duchateau JL, et al. Control of contact resistance by strand surface coating in 36-strand NbTi CICCs. Cryogenics. 2001;**41**(1):1-7

[31] Khoshnevisan M, Pratt WP Jr, Schroeder PA, et al. Low-temperature resistivity of silver. Journal of Physics F: Metal Physics. 1979;**9**(1):L1

[32] Martin DL. Low-temperature electrical resistivity and superconducting transition temperature of indium-manganese alloys. Physical Review. 1965;**138**(2A):A464

[33] I. Corporation. Physical Constants of Pure Indium. Available from: http://www.indium.com/metals/indium/physical-constants. [Accessed: December 12, 2017]

[34] Ciazynski D, Martinez A. Electrical and thermal designs and analyses of joints for the ITER PF coils. IEEE Transactions on Applied Superconductivity. 2002;**12**(1):538-542

[35] Zani L, Ciazynski D, Heller R, et al. Study of current distribution in ITER TFMC NbTi Busbar III. IEEE Transactions on Applied Superconductivity. 2006;**16**(2): 864-867

[36] Zanino R, Bessette D, Richard LS. Quench analysis of an ITER TF coil. Fusion Engineering and Design. 2010; **85**(5):752-760

[37] Li S, Wu Y, Liu B, et al. Current sharing temperature test and simulation with GANDALF code for ITER PF2 conductor sample. Plasma Science and Technology. 2011;**13**(5):627

[38] Bottura L, Rosso C. Finite element simulation of steady state and transient forced convection in superfluid helium. International Journal for Numerical Methods in Fluids. 1999;**30**(8): 1091-1108

[39] Wang Q, Kim K, Yoon CS. Numerical model for thermal hydraulic analysis in cable-in-conduit-conductors. KSME international journal. 2000;**14**(9): 985-996

[40] Huang H, Wang Q. Heat Transfer Finite Element Analysis. Beijing: China Science publishing & Media Ltd.; 2011

[41] Miyoshi Y, Wessel WAJ, Krooshoop JG, et al. AC Loss Measurement with Transverse Load Cycles in Twente Press on Hitachi-81JNC002-S4T1. Intermediate Report UT-IO-2011-516. University of Twente; 2011

[42] Marinucci C, Savoldi L, Zannino R. Stability analysis of the ITER TF and CS conductors using the code Gandalf. IEEE Transactions on Applied Superconductivity. 1999;**9**(2):612-615

[43] Fu M, Xu X, Jiao Z, et al. Minimum quench energy and normal zone propagation velocity in MgB2 superconducting tape. Physica C: Superconductivity. 2004;**402**(3): 234-238

[44] Wilson MN, Wolf R. Calculation of minimum quench energies in Rutherford cables. IEEE Transactions on Applied Superconductivity. 1997;**7**(2): 950-953

[45] Wilson MN. Computation of Minimum Quench Energies in LHC Cables. Geneva, Switzerland: CERN; 1997

[46] Ghosh AK, Sampson WB, Bauer P, et al. Minimum quench energy measurements on single strands for LHC main magnets. IEEE Transactions on Applied Superconductivity. 1999;**9**(2): 252-256

[47] Calvi M, Busbar ITER. Design Studies, Swiss Federal Institute of Technology. V1.3, Lausanne: Center for Research in Plasma Physics; 2010

[48] Bauer P, Bessette D, Calvi M, Nannini M. ITER Busbar Thermohydraulic Anal-Ysis, ITER IDM 4D5SM9

[49] Zanino R, Bottura L, Marinucci C. A comparison between 1-and 2-fluid simulations of the QUELL conductor. IEEE Transactions on Applied Superconductivity. 1997;**7**(2):493-496